Zn^{2+} is Essential for Ca^{2+} Oscillations in Mouse Eggs

Hiroki Akizawa[1], Emily Lopes[1,2], Rafael A. Fissore[1*]

[1]Department of Veterinary and Animal Sciences, University of Massachusetts Amherst, 661 North Pleasant Street, Amherst, Massachusetts, 01003, United States.
[2]Molecular and Cellular Biology Graduate Program, University of Massachusetts, Amherst, Massachusetts, 01003, United States.

Running Title: Labile Zn^{2+} and Ca^{2+} release

Key Words: Fertilization, mammals, Ca^{2+}, IP_3R1, oocytes, eggs, sperm, divalent cations, chelators

[*]Author for correspondence (rfissore@umass.edu)

*Rafael A. Fissore
661 North Pleasant Street
ISB-427A
Department of Veterinary and Animal Science
University of Massachusetts, Amherst, 01003
Phone:413-687-5773
Email: rfissore@umass.edu

Abstract

Changes in the intracellular concentration of free calcium (Ca^{2+}) underpin egg activation and initiation of development in animals and plants. In mammals, the Ca^{2+} release is periodical, known as Ca^{2+} oscillations, and mediated by the type 1 inositol 1,4,5-trisphosphate receptor (IP_3R1). Another divalent cation, zinc (Zn^{2+}), increases exponentially during oocyte maturation and is vital for meiotic transitions, arrests, and polyspermy prevention. It is unknown if these pivotal cations interplay during fertilization. Here, using mouse eggs, we showed that basal concentrations of labile Zn^{2+} are indispensable for sperm-initiated Ca^{2+} oscillations because Zn^{2+}-deficient conditions induced by cell-permeable chelators abrogated Ca^{2+} responses evoked by fertilization and other physiological and pharmacological agonists. We also found that chemically- or genetically generated eggs with lower levels of labile Zn^{2+} displayed reduced IP_3R1 sensitivity and diminished ER Ca^{2+} leak despite the stable content of the stores and IP_3R1 mass. Resupplying Zn^{2+} restarted Ca^{2+} oscillations, but excessive Zn^{2+} prevented and terminated them, hindering IP_3R1 responsiveness. The findings suggest that a window of Zn^{2+} concentrations is required for Ca^{2+} responses and IP_3R1 function in eggs, ensuring optimal response to fertilization and egg activation.

Introduction

Vertebrate eggs are arrested at the metaphase stage of the second meiosis (MII) when ovulated because they have an active Cdk1/cyclin B complex and inactive APC/C^{Cdc20} (Heim et al., 2018). Release from MII initiates egg activation, the first hallmark of embryonic development (Ducibella et al., 2002; Schultz and Kopf, 1995). The universal signal of egg activation is an increase in the intracellular concentration of calcium (Ca^{2+}) (Ridgway et al., 1977; Stricker, 1999). Ca^{2+} release causes the inactivation of the APC/C inhibitor Emi2, which enhances cyclin B degradation and induces meiotic exit (Lorca et al., 1993; Shoji et al., 2006; Suzuki et al., 2010a). In mammals, the stereotypical fertilization Ca^{2+} signal, oscillations, consists of transient but periodical Ca^{2+} increases that promote progression into interphase (Deguchi et al., 2000; Miyazaki et al., 1986). The sperm-borne Phospholipase C zeta1 (PLCζ) persistently stimulates the production of inositol 1,4,5-trisphosphate (IP_3) (Matsu-ura et al., 2019; Saunders et al., 2002; Wu et al., 2001) that binds its cognate receptor in the endoplasmic reticulum (ER), IP_3R1 and causes Ca^{2+} release from the egg's main Ca^{2+} reservoir (Wakai et al., 2019). The intake of extracellular Ca^{2+} via plasma membrane channels and transporters ensures the persistence of the oscillations (Miao et al., 2012; Stein et al., 2020; Wakai et al., 2019, 2013).

Before fertilization, maturing oocytes undergo cellular and biochemical modifications (see for review (Ajduk et al., 2008)). The nucleus of immature oocytes, known as the germinal vesicle (GV), undergoes the breakdown of its envelope marking the onset of maturation and setting in motion a series of cellular events that culminate with the release of the first polar body, the correct ploidy for fertilization, and re-arrest at MII (Eppig, 1996). Other organelles are also reorganized, such as cortical granules migrate to the cortex for exocytosis and polyspermy block, mitochondria undergo repositioning, and the cytoplasm's redox state becomes progressively reduced to promote the exchange of the sperm's protamine load (Liu, 2011; Perreault et al., 1988; Wakai et al., 2014). Wide-ranging adaptations also occur in the Ca^{2+} release machinery to produce timely and protracted Ca^{2+} oscillations following sperm entry (Fujiwara et al., 1993; Lawrence et al., 1998), including the increase in the content of the Ca^{2+} stores, ER reorganization with cortical cluster formation, and increased IP_3R1 sensitivity (Lee et al., 2006; Wakai et al., 2012). The total intracellular levels of zinc (Zn^{2+}) also remarkably increase during maturation, amounting to a 50% rise, which is necessary for oocytes to proceed to the telophase I of meiosis and beyond (Kim et al., 2010). Remarkably, after fertilization, Zn^{2+} levels need to decrease, as Emi2 is a Zn^{2+}-associated molecule, and high Zn^{2} levels prevent MII exit (Bernhardt et al., 2012; Shoji et al., 2014; Suzuki et al., 2010b). Following the initiation of Ca^{2+} oscillations, approximately 10 to 20% of the Zn^{2+} accrued during maturation is ejected during the Zn^{2+} sparks, a conserved event in vertebrates and invertebrate species (Converse and Thomas, 2020; Kim et al., 2011; Mendoza et al., 2022; Que et al., 2019; Seeler et al., 2021; Tokuhiro and Dean, 2018; Wozniak et al., 2020; Zhang et al., 2016). The use of Zn^{2+} chelators such as N,N,N,N-tetrakis (2-pyridinylmethyl)-1,2-ethylenediamine (TPEN) to create Zn^{2+}-deficient conditions buttressed the importance of Zn^{2+} during meiotic transitions (Kim et al., 2010; Suzuki et al., 2010b). However, whether the analogous dynamics of Ca^{2+} and Zn^{2+} during maturation imply crosstalk and Zn^{2+} levels modulate Ca^{2+} release during fertilization is unknown.

IP_3Rs are the most abundant intracellular Ca^{2+} release channel in non-muscle cells (Berridge, 2016). They form a channel by assembling into tetramers with each subunit of ~270kDa MW (Taylor and Tovey, 2010). Mammalian eggs express the type I IP_3R, the most widespread isoform (Fissore et al., 1999; Parrington et al., 1998). IP_3R1 is essential for egg activation because its inhibition precludes Ca^{2+} oscillations (Miyazaki and Ito, 2006; Miyazaki et al., 1992; Xu et al., 2003). Myriad and occasionally cell-specific factors influence Ca^{2+} release through the IP_3R1 (Taylor and Tovey, 2010). For example, following fertilization, IP_3R1 undergoes ligand-induced degradation caused by

96 the sperm-initiated long-lasting production of IP_3 that effectively reduces the IP_3R1 mass
97 (Brind et al., 2000; Jellerette et al., 2000). Another regulatory mechanism is Ca^{2+}, a
98 universal cofactor, which biphasically regulates IP_3Rs' channel opening (Iino, 1990; Jean
99 and Klee, 1986), congruent with several Ca^{2+} and calmodulin binding sites on the
100 channel's sequence (Sienaert et al., 1997; Sipma et al., 1999). Notably, Zn^{2+} may also
101 participate in IP_3R1 regulation. Recent studies using electron cryomicroscopy (cryoEM),
102 a technique that allows peering into the structure of IP_3R1 with a near-atomic resolution,
103 have revealed that a helical linker (LNK) domain near the C-terminus mediates the
104 coupling between the N- and C-terminal ends necessary for channel opening (Fan et al.,
105 2015). The LNK domain contains a putative Zinc-finger motif proposed to be vital for
106 IP_3R1 function (Fan et al., 2015; Paknejad and Hite, 2018). Therefore, the exponential
107 increase in Zn^{2+} levels in maturing oocytes, besides its essential role in meiosis
108 progression, may optimize the IP_3R1 function, revealing hitherto unknown cooperation
109 between these cations during fertilization.
110 Here, we examined whether crosstalk between Ca^{2+} and Zn^{2+} is required to
111 initiate and sustain Ca^{2+} oscillations and maintain Ca^{2+} store content in MII eggs. We
112 found that Zn^{2+}-deficient conditions inhibited Ca^{2+} release and oscillations without
113 reducing Ca^{2+} stores, IP_3 production, IP_3R1 expression, or altering the viability of eggs or
114 zygotes. We show instead that Zn^{2+} deficiency impaired IP_3R1 function and lessened the
115 receptor's ability to gate Ca^{2+} release out of the ER. Remarkably, resupplying Zn^{2+} re-
116 established the oscillations interrupted by low Zn^{2+}, although persistent increases in
117 intracellular Zn^{2+} were harmful, disrupting the Ca^{2+} responses and preventing egg
118 activation. Together, the results show that besides contributing to oocyte maturation, Zn^{2+}
119 has a central function in Ca^{2+} homeostasis such that optimal Zn^{2+} concentrations ensure
120 IP_3R1 function and the Ca^{2+} oscillations required for initiating embryo development.
121
122 **Results**
123 ***TPEN dose-dependently lowers intracellular Zn^{2+} and inhibits sperm-initiated Ca^{2+}***
124 ***oscillations.***
125 TPEN is a cell-permeable, non-specific chelator with a high affinity for transition
126 metals widely used to study their function in cell physiology (Arslan et al., 1985; Lo et
127 al., 2020). Mouse oocytes and eggs have exceedingly high intracellular concentrations of
128 Zn^{2+} (Kim et al., 2011, 2010), and the TPEN-induced defects in the progression of meiosis
129 have been ascribed to its chelation (Bernhardt et al., 2011; Kim et al., 2010). In support
130 of this view, the Zn^{2+} levels of cells showed acute reduction after TPEN addition, as
131 reported by indicators such as FluoZin-3 (Arslan et al., 1985; Gee et al., 2002; Suzuki et

132 al., 2010b). Studies in mouse eggs also showed that the addition of low μM (40-100)
133 concentrations of TPEN disrupted Ca^{2+} oscillations initiated by fertilization or $SrCl_2$
134 (Lawrence et al., 1998; Suzuki et al., 2010b), but the mechanism(s) and target(s) of the
135 inhibition remained unknown. To gain insight into this phenomenon, we first performed
136 dose-titration studies to determine the effectiveness of TPEN in lowering Zn^{2+} in eggs.
137 The addition of 2.5 μM TPEN protractedly reduced Zn^{2+} levels, whereas 5 and 10 μM
138 TPEN acutely and persistently reduced FluoZin-3 fluorescence (**Fig. 1A)**. These
139 concentrations of TPEN are higher than the reported free Zn^{2+} concentrations in cells, but
140 within range of those of found in typical culture conditions (Lo et al., 2020; Qin et al.,
141 2011). We next determined the concentrations of TPEN required to abrogate fertilization-
142 initiated oscillations. Following intracytoplasmic sperm injection (ICSI), we monitored
143 Ca^{2+} responses while increasing TPEN concentrations. As shown in **Fig. 1B**, 5 and 10 μM
144 TPEN effectively blocked ICSI-induced Ca^{2+} oscillations in over half of the treated cells,
145 and the remaining eggs, after a prolonged interval, resumed lower-frequency rises (**Fig.**
146 **1B**-center panels). Finally, 50 μM or greater concentrations of TPEN permanently
147 blocked these oscillations (**Fig. 1B**-right panel). It is noteworthy that at the time of
148 addition, TPEN concentrations of 5 μM or above induce a sharp drop in basal Fura-2
149 F340/ F380 ratios, consistent with Fura-2's high affinity for Zn^{2+} (Snitsarev et al., 1996).
150 We next used membrane-permeable and -impermeable chelators to assess
151 whether TPEN inhibited Ca^{2+} oscillations by chelating Zn^{2+} from intracellular or
152 extracellular compartments. The addition of the high-affinity but cell-impermeable Zn^{2+}
153 chelators DTPA and EDTA neither terminated nor temporarily interrupted ICSI-induced
154 Ca^{2+} oscillations (**Fig. 1C**), although protractedly slowed them down, possibly because
155 of chelation and lowering of external Ca^{2+} (**Fig. 1C**). These results suggest that chelation
156 of external Zn^{2+} does not affect the continuation of oscillations. We cannot determine that
157 EDTA successfully chelated all external Zn^{2+}, but the evidence that the addition of EDTA
158 to the monitoring media containing cell impermeable FluoZin-3 caused a marked
159 reduction in fluorescence, suggests that a noticeable fraction of the available Zn^{2+} was
160 sequestered (**Supplementary Fig. 1A**). Similarly, injection of m*Plcζ* mRNA in eggs
161 incubated in Ca^{2+} and Mg^{2+}-free media supplemented with EDTA, to maximize the
162 chances of chelation of external Zn^{2+}, initiated low-frequency but persistent oscillations,
163 and addition of Ca^{2+} and Mg^{2+} restored the physiological periodicity (**Supplementary Fig.**
164 **1B)**. Lastly, another Zn^{2+}-permeable chelator, TPA, blocked the ICSI-initiated Ca^{2+}
165 oscillations but required higher concentrations than TPEN (**Fig. 1D**). Collectively, the
166 data suggest that basal levels of labile internal Zn^{2+} are essential to sustain the
167 fertilization-initiated Ca^{2+} oscillations in eggs.

168 We next evaluated whether Zn^{2+} depletion prevented the completion of meiosis
169 and pronuclear (PN) formation. To this end, ICSI-fertilized eggs were cultured in the
170 presence of 10 μM TPEN for 8h, during which the events of egg activation were examined
171 (**Fig. 1E and Table 1**). All fertilized eggs promptly extruded second polar bodies
172 regardless of treatment (**Fig. 1E**). TPEN, however, impaired PN formation, and by 4- or
173 7-h post-ICSI, most treated eggs failed to show PNs, unlike controls (**Fig. 1E and Table**
174 **1**). Together, these results demonstrate that depletion of Zn^{2+} terminates Ca^{2+} oscillations
175 and delays or prevents events of egg activation, including PN formation.
176
177 ***TPEN is a universal inhibitor of Ca^{2+} oscillations in eggs.***
178 Mammalian eggs initiate Ca^{2+} oscillations in response to numerous stimuli and
179 conditions (Miyazaki and Ito, 2006; Wakai and Fissore, 2013). Fertilization and its release
180 of PLCζ stimulate the phosphoinositide pathway, producing IP_3 and Ca^{2+} oscillations
181 (Miyazaki, 1988; Saunders et al., 2002). Neurotransmitters such as acetylcholine (Ach)
182 and other G-protein coupled receptor agonists engage a similar mechanism (Dupont et al.,
183 1996; Kang et al., 2003), although in these cases, IP_3 production occurs at the plasma
184 membrane and is short-lived (Kang et al., 2003; Swann and Parrington, 1999). Agonists
185 such as $SrCl_2$ and thimerosal generate oscillations by sensitizing IP_3R1 without producing
186 IP_3. The mechanism(s) of $SrCl_2$ is unclear, although its actions are reportedly directly on
187 the IP_3R1 (Hajnóczky and Thomas, 1997; Hamada et al., 2003; Nomikos et al., 2015,
188 2011; Sanders et al., 2018). Thimerosal oxidizes dozens of thiol groups in the receptor,
189 which enhances the receptor's sensitivity and ability to release Ca^{2+} (Bootman et al.,
190 1992; Evellin et al., 2002; Joseph et al., 2018). We took advantage of the varied points at
191 which the mentioned agonists engage the phosphoinositide pathway to examine TPEN's
192 effectiveness in inhibiting their effects. m*Plcζ* mRNA injection, like fertilization, induces
193 persistent Ca^{2+} oscillations, although m*Plcζ*'s tends to be more robust. Consistent with
194 this, the addition of 10 and 25 μM TPEN transiently interrupted or belatedly terminated
195 oscillations, whereas 50 μM acutely stopped all responses (**Fig. 2A**). By contrast, $SrCl_2$-
196 initiated rises were the most sensitive to Zn^{2+}-deficient conditions, with 2.5 μM TPEN
197 nearly terminating all oscillations that 5 μM did (**Fig. 2B**). TPEN was equally effective
198 in ending the Ach-induced Ca^{2+} responses (**Fig. 2C**), but curbing thimerosal responses
199 required higher concentrations (**Fig. 2D**). Lastly, we ruled out that downregulation of
200 IP_3R1 was responsible for the slow-down or termination of the oscillations by TPEN. To
201 accomplish this, we examined the IP_3R1 mass in eggs (Jellerette et al., 2004) with and
202 without TPEN supplementation and injection of m*Plcζ* mRNA. By 4h post-injection,
203 PLCζ induced the expected down-regulation of IP_3R1 reactivity, whereas was

204 insignificant in TPEN-treated and *Plcζ* mRNA-injected eggs, as it was in uninjected
205 control eggs (**Fig. 2F**). These findings together show that Zn^{2+} deficiency inhibits the
206 IP_3R1-mediated Ca^{2+} oscillations independently of IP_3 production or loss of receptor,
207 suggesting a role of Zn^{2+} on IP_3R1 function (**Fig. 2E**).
208
209 ***Zn^{2+} depletion reduces IP_3R1-mediated Ca^{2+} release.***
210 To directly assess the inhibitory effects of TPEN on IP_3R1 function, we used caged
211 IP_3 (cIP_3) that, after short UV pulses, releases IP_3 into the ooplasm (Wakai et al., 2012;
212 Walker et al., 1987). To exclude the possible contribution of external Ca^{2+} to the responses,
213 we performed the experiments in Ca^{2+}-free media. In response to sequential cIP_3 release
214 5 min apart, control eggs displayed corresponding Ca^{2+} rises that occasionally
215 transitioned into short-lived oscillations (**Fig. 3A**). The addition of TPEN after the third
216 cIP_3 release prevented the subsequent Ca^{2+} response and prematurely terminated the in-
217 progress Ca^{2+} rises (**Fig. 3B and inset)**. Pre-incubation of eggs with TPEN precluded
218 cIP_3-induced Ca^{2+} release, even after 5 sec UV exposure (**Fig. 3C**). The addition of excess
219 $ZnSO_4$ (100 μM) overcame TPEN's inhibitory effects only if added before **(Fig. 3E)** and
220 not after the addition of TPEN **(Fig. 3D)**. Similar concentrations of $MgCl_2$ or $CaCl_2$ failed
221 to reverse TPEN effects **(Fig. 3F, G)**. Together, the results show that Zn^{2+} is required for
222 IP_3R1-mediated Ca^{2+} release downstream of IP_3 production, appearing to interfere with
223 receptor gating, as suggested by TPEN's rapid termination of in-progress Ca^{2+} rises and
224 ongoing oscillations.
225 ERp44 is an ER luminal protein of the thioredoxin family that interacts with the
226 IP_3R1, reportedly inhibiting its ability to mediate Ca^{2+} release (Higo et al., 2005). The
227 localization of ERp44 in the ER-Golgi intermediate compartment of somatic cells
228 correlates with Zn^{2+}'s availability and changes dramatically after TPEN treatment (Higo
229 et al., 2005; Watanabe et al., 2019). To rule out the possibility that TPEN suppresses the
230 function of IP_3R1 by modifying the subcellular distribution of ERp44, we overexpressed
231 ERp44 by injecting HA tagged-*Erp44* mRNA into MII eggs and monitored the effect on
232 Ca^{2+} release. TPEN did not alter the localization of ERp44 (**Supplementary Fig. 2A**),
233 and overexpression of ERp44 modified neither the Ca^{2+} oscillations induced by agonists
234 (**Supplementary Fig. 2B**) nor the effectiveness of TPEN to block them (data not shown).
235 Thus, TPEN and Zn^{2+} deficiency most likely inhibits Ca^{2+} release by directly interfering
236 with IP_3R1 function rather than modifying this particular regulator.
237
238 ***Zn^{2+} depletion diminishes the ER Ca^{2+} leak and increases Ca^{2+} store content.***

239 Our above cIP_3 results that TPEN inhibited IP_3R1-mediated Ca^{2+} release and
240 interrupted in-progress Ca^{2+} rises despite the presence of high levels of environmental IP_3
241 suggest its actions are probably independent of IP_3 binding, agreeing with an earlier report
242 showing that TPEN did not modify IP_3's affinity for the IP_3R (Richardson and Taylor,
243 1993). Additionally, the presence of a Zn^{2+}-binding motif near the C-term cytoplasmic
244 domain of the IP_3R1's channel, which is known to influence agonist-induced IP_3R1 gating
245 (Fan et al., 2015), led us to posit and examine that Zn^{2+} deficiency may be disturbing Ca^{2+}
246 release to the cytosol and out of the ER. To probe this possibility, we queried if pre-
247 treatment with TPEN inhibited Ca^{2+} release through IP_3R1. We first used Thapsigargin
248 (Tg), a Sarcoplasmic/ER Ca^{2+} ATPase pump inhibitor (Thastrup et al., 1990) that unmasks
249 a constitutive Ca^{2+} leak out of the ER (Lemos et al., 2021); in eggs, we have demonstrated
250 it is mediated at least in part by IP_3R1 (Wakai et al., 2019). Treatment with TPEN for 15
251 min slowed the Tg-induced Ca^{2+} leak into the cytosol, resulting in delayed and lowered
252 amplitude Ca^{2+} responses (**Fig. 4A;** $P<0.05$). To test whether the reduced response to Tg
253 means that TPEN prevented the complete response of Tg, leaving a temporarily increased
254 Ca^{2+} content in the ER, we added the Ca^{2+} ionophore ionomycin (Io), which empties all
255 stores independently of IP_3Rs. Io-induced Ca^{2+} responses were 3.3-fold greater in TPEN-
256 treated cells, supporting the view that TPEN interferes with the ER Ca^{2+} leak **(Fig. 4A;** P
257 < 0.05). We further evaluated this concept using *in vitro* aged eggs that often display
258 reduced Ca^{2+} store content than freshly collected counterparts (Abbott et al., 1998). After
259 culturing eggs in the presence or absence of TPEN for 2h, we added Io during Ca^{2+}
260 monitoring, which in TPEN-treated eggs induced bigger Ca^{2+} rises than in control eggs
261 **(Fig. 4B;** $P<0.05$**)**. We confirmed that this effect was independent of IP_3R1 degradation
262 because TPEN did not change IP_3R1 reactivity in unfertilized eggs (**Fig. 4C**; $P<0.05$).
263 Next, we used the genetically encoded FRET sensor D1ER (Palmer et al., 2004) to
264 assess the TPEN's effect on the ER's relative Ca^{2+} levels changes following the additions
265 of Tg or Ach. TPEN was added 10 min before 10 μM Tg or 50 μM Ach, and we
266 simultaneously monitored changes in cytosolic and intra-ER Ca^{2+} (**Fig. 4D, E**). For the
267 first three min, the Tg-induced decrease in Ca^{2+}-ER was similar between groups. However,
268 while the drop in Ca^{2+} content continued in control eggs, in TPEN-treated eggs, it came
269 to an abrupt halt, generating profound differences between the two groups (**Fig. 4D;** P
270 <0.05). TPEN had even more pronounced effects following the addition of Ach, leading
271 to a reduced- and prematurely terminated- Ca^{2+} release from the ER in treated eggs (**Fig.**
272 **4E;** $P<0.05$).
273 Lastly, we sought to use a cellular model where low labile Zn^{2+} occurred without
274 pharmacology. To this end, we examined a genetic model where the two non-selective

275 plasma membrane channels that could influx Zn^{2+} in maturing oocytes have been deleted
276 (Bernhardt et al., 2017; Carvacho et al., 2016, 2013), namely, the transient receptor
277 potential melastatin-7 (TRPM7) and TRP vanilloid 3 (TRPV3), both members of the TRP
278 superfamily of channels (Wu et al., 2010). We found that eggs from double knockout
279 females (dKOs) had lower levels of labile Zn^{2+} (**Fig. 4F**), and the addition of Tg revealed
280 an expanded Ca^{2+} store content in these eggs vs. control WT eggs (**Fig. 4G**). Remarkably,
281 in dKO eggs, the Ca^{2+} rise induced by Tg showed a shoulder or inflection point before
282 the peak delaying the time to peak (**Fig. 4G**, **inset**; P <0.001). These results in dKO eggs
283 show a changed dynamic of the Tg-induced Ca^{2+} release, suggesting that lower levels of
284 labile Zn^{2+} modify ER Ca^{2+} release independently of chelators.
285
286 ***Ca^{2+} oscillations in eggs occur within a window of Zn^{2+} concentrations.***
287 We next examined if resupplying Zn^{2+} could restart the Ca^{2+} oscillations
288 terminated by Zn^{2+} depletion. Zn pyrithione (ZnPT) rapidly increases cellular Zn^{2+} upon
289 extracellular addition (Barnett et al., 1977; Robinson, 1964). Dose titration studies and
290 imaging fluorimetry revealed that 0.01 μM ZnPT caused subtle and protracted increases
291 in Zn^{2+} levels, whereas 0.1 μM ZnPT caused rapid increases in eggs' Zn^{2+} baseline (**Fig.**
292 **5A**). We induced detectable Ca^{2+} oscillations by injection of m*Plcζ* mRNA followed by
293 50 μM TPEN (**Fig. 5B**), which terminated them. After 30 min, we added 0.1 μM ZnPT,
294 and within 15 min the oscillations restarted in most TPEN-treated eggs (**Fig. 5C**). We
295 repeated this approach using Thimerosal (**Fig. 5D, E**). Adding 0.1 μM ZnPT did not
296 restore the Ca^{2+} oscillations retrained by TPEN, but 0.5 μM ZnPT did so (**Fig. 5E**). These
297 results demonstrate that Zn^{2+} plays a pivotal, enabling role in the generation of Ca^{2+}
298 oscillations in mouse eggs.
299
300 ***Excessive intracellular Zn^{2+} inhibits Ca^{2+} oscillations.***
301 Zn^{2+} is necessary for diverse cellular functions, consistent with numerous amino
302 acids and proteins capable of binding Zn^{2+} within specific and physiological ranges (Pace
303 and Weerapana, 2014). Excessive Zn^{2+}, however, can cause detrimental effects on cells
304 and organisms (Broun et al., 1990; Hara et al., 2022; Sikora and Ouagazzal, 2021).
305 Consistent with the deleterious effects of Zn^{2+}, a previous study showed that high
306 concentrations of ZnPT, ~50 μM, prevented $SrCl_2$-induced egg activation and initiation
307 of development (Bernhardt et al., 2012; Kim et al., 2011). We examined how ZnPT and
308 excessive Zn^{2+} levels influence Ca^{2+} oscillations. Our conditions revealed that pre-
309 incubation or continuous exposure to 0.1 μM or 1.0 μM ZnPT delayed or prevented egg
310 activation induced by m*Plcζ* mRNA injection (**Supplementary Fig. 3**). We used these

ZnPT concentrations to add it into ongoing oscillations induced by ICSI and monitored the succeeding Ca^{2+} responses. The addition of 0.05 to 10 μM ZnPT caused an immediate elevation of the basal levels of Fura-2 and termination of the Ca^{2+} oscillations (**Fig. 6A-D)**. m*Plcζ* mRNA-initiated Ca^{2+} responses were also interrupted by adding 0.1 μM ZnPT, whereas untreated eggs continued oscillating (**Fig. 6E, F**). ZnPT also inhibited IP_3R1-mediated Ca^{2+} release triggered by cIP_3, suggesting that excessive Zn^{2+} directly inhibits IP_3R1 function (**Fig. 6G)**.

A noticeable feature of ZnPT is the increased basal ratios of Fura-2 AM. These changes could reflect enhanced IP_3R1 function and increased basal Ca^{2+} concentrations caused by Zn^{2+} stimulation of IP_3R1. This seems unlikely, however, because extended elevated cytosolic Ca^{2+} would probably induce cellular responses, such as the release of the second polar body, egg fragmentation, or cell death, neither of which happened. It might reflect, instead, Fura-2's ability to report changes in Zn^{2+} levels, which seemed the case because the addition of TPEN lowered fluorescence without restarting the Ca^{2+} oscillations (**Fig. 6F**). To ensure the impact of ZnPT abolishing Ca^{2+} oscillations was not an imaging artifact obscuring ongoing rises, we simultaneously monitored cytoplasmic and ER Ca^{2+} levels with Rhod-2 and D1ER, respectively. This approach allowed synchronously observing Ca^{2+} changes in both compartments that should unfold in opposite directions. In control, uninjected eggs, the fluorescent values for both reporters remained unchanged during the monitoring period, whereas in m*Plcζ* mRNA-injected eggs, the reporters' signals displayed simultaneous but opposite changes, as expected (**Fig. 6H, I**). The addition of ZnPT in uninjected eggs rapidly increased Rhod-2 signals but not D1ER's, which was also the case in oscillating eggs, as the addition of ZnPT did not immediately alter the dynamics of the ER's Ca^{2+} release, suggesting D1ER faithfully reports in Ca^{2+} changes but cannot detect changes in Zn^{2+} levels, at least to this extent; ZnPT progressively caused fewer and lower amplitude changes in D1ER fluorescence, consistent with the diminishing and eventual termination of the Ca^{2+} oscillations. Noteworthy, in these eggs, the basal D1ER fluorescent ratio remained unchanged after ZnPT, demonstrating its unresponsiveness to Zn^{2+} changes of this magnitude. The ZnPT-induced increases in Rhod-2 fluorescence without concomitant changes in D1ER values suggest that the changes in the dyes' fluorescence do not represent an increase in basal Ca^{2+} and, more likely, signal an increase in intracellular Zn^{2+}. We confirmed that both reporters were still in working order, as the addition of Io triggered Ca^{2+} changes detected by both reporters (**Fig. 6H, I**).

Discussion

347 The present study demonstrates that appropriate levels of labile Zn^{2+} are essential
348 for initiating and maintaining IP_3R1-mediated Ca^{2+} oscillations in mouse eggs regardless
349 of the initiating stimuli. Both deficient and excessive Zn^{2+} compromise IP_3R1 sensitivity,
350 diminishing and mostly terminating Ca^{2+} oscillations. The results demonstrate that IP_3R1
351 and Zn^{2+} act in concert to modulate Ca^{2+} signals, revealing previously unexplored
352 crosstalk between these ions at fertilization (**Fig. 7**).
353 Zn^{2+} is an essential micronutrient for living organisms (Kaur et al., 2014) and is
354 required for various cellular functions, such as proliferation, transcription, and
355 metabolism (Lo et al., 2020; Maret and Li, 2009; Yamasaki et al., 2007). Studies using
356 Zn^{2+} chelators have uncovered what appears to be a cell-specific, narrow window of Zn^{2+}
357 concentrations needed for cellular proliferation and survival (Carraway and Dobner,
358 2012; Lo et al., 2020). Further, TPEN appeared especially harmful, and in a few cell lines,
359 even low doses provoked oxidative stress, DNA fragmentation, and apoptosis (Mendivil-
360 Perez et al., 2012). We show here that none of the Zn^{2+} chelators, permeable or
361 impermeable, affected cell viability within our experimental observations, confirming
362 findings from previous studies that employed high concentrations of TPEN to interrupt
363 the Ca^{2+} oscillations (Lawrence et al., 1998) or inducing egg activation of mouse eggs
364 (Suzuki et al., 2010b). Our data demonstrating that ~2.5 μM is the threshold concentration
365 of TPEN in eggs that first causes noticeable changes in basal Zn^{2+}, as revealed by FluoZin,
366 is consistent with the ~2 to 5-μM Zn^{2+} concentrations in most culture media without
367 serum supplementation (Lo et al., 2020), and with the ~100 pM basal Zn^{2+} in cells (Qin
368 et al., 2011). Lastly, the effects on Ca^{2+} release observed here with TPEN and other
369 chelators were due to the chelation of Zn^{2+}, as pretreatment with $ZnSO_4$ but not with equal
370 or greater concentrations of $MgCl_2$ or $CaCl_2$ rescued the inhibition of the responses, which
371 is consistent with results by others (Kim et al., 2010; Lawrence et al., 1998).
372 To identify how Zn^{2+} deficiency inhibits Ca^{2+} release in eggs, we induced Ca^{2+}
373 oscillations using various stimuli and tested the effectiveness of membrane-permeable
374 and impermeable chelators to abrogate them. Chelation of extracellular Zn^{2+} failed to
375 terminate the Ca^{2+} responses, whereas membrane-permeable chelators did, pointing to
376 intracellular labile Zn^{2+} levels as essential for Ca^{2+} release. All agonists used here were
377 susceptible to inhibition by TPEN, whether their activities depended on IP_3 production or
378 allosterically induced receptor function, although the effective TPEN concentrations
379 varied across stimuli. Some agents, such as m*Plcζ* mRNA or thimerosal, required higher
380 concentrations than $SrCl_2$, Ach, or cIP_3. The reason underlying the different agonists'
381 sensitivities to TPEN will require additional research, but the persistence of IP_3
382 production or change in IP_3R1 structure needed to induce channel gating might explain

383 it. However, the universal abrogation of Ca^{2+} oscillations by TPEN supports the view
384 drawn from cryo-EM-derived IP_3R1 models that signaling molecules can allosterically
385 induce channel gating from different starting positions in the receptor by mechanically
386 coupling the binding effect to the ion-conducting pore in the C-terminal end of IP_3R (Fan
387 et al., 2015). The cytosolic C-terminal domain of each IP_3R1 subunit is alongside the IP_3-
388 binding domain of another subunit and, therefore, well positioned to sense IP_3 binding
389 and induce channel gating (Fan et al., 2015). Within each subunit, the LNK domain, which
390 contains a Zn^{2+}-finger motif (Fan et al., 2015), connects the opposite domains of the
391 molecule. Although there are no reports regarding the regulation of IP_3R1 sensitivity by
392 Zn^{2+}, such evidence exists for RyRs (Woodier et al., 2015), which also display a conserved
393 Zn^{2+}-finger motif (des Georges et al., 2016). Lastly, mutations of the two Cys or two His
394 residues of this motif, without exception, resulted in inhibition or inactivation of the IP_3R1
395 channel (Bhanumathy et al., 2012; Uchida et al., 2003). These results are consistent with
396 the view that the C-terminal end of IP_3Rs plays a dominant role in channel gating
397 (Bhanumathy et al., 2012; Uchida et al., 2003). We propose that TPEN inhibits Ca^{2+}
398 oscillations in mouse eggs because chelating Zn^{2+} interferes with the function of the LNK
399 domain and its Zn^{2+}-finger motif proposed role on the mechanical coupling induced by
400 agonist binding to the receptor that propagates to the pore-forming region and required to
401 gate the channel's ion-pore (Fan et al., 2022, 2015).
402 In support of this possibility, TPEN-induced Zn^{2+} deficient conditions altered the
403 Ca^{2+}-releasing kinetics in resting eggs or after fertilization. Tg increases intracellular Ca^{2+}
404 by inhibiting the SERCA pump (Thastrup et al., 1990) and preventing the reuptake into
405 the ER of the ebbing Ca^{2+} during the basal leak. Our previous studies showed that the
406 downregulation of IP_3R1 diminishes the leak, suggesting it occurs through IP_3R1 (Wakai
407 and Fissore, 2019). Consistent with this view, TPEN pre-treatment delayed the Ca^{2+}
408 response induced by Tg, implying that Zn^{2+} deficiency hinders Ca^{2+} release through IP_3R1.
409 An expected consequence would be increased Ca^{2+} content in the ER after Tg. Io that
410 mobilizes Ca^{2+} independently of IP_3Rs (Toeplitz et al., 1979) induced enhanced responses
411 in TPEN-treated eggs vs. controls, confirming the accumulation of Ca^{2+}- ER in Zn^{2+}
412 deficient conditions. We demonstrated that this accumulation is due to hindered emptying
413 of the Ca^{2+} ER evoked by agonists in Zn^{2+}-deficient environments, resulting in reduced
414 cytosolic Ca^{2+} increases, as IP_3R1 is the pivotal intermediary channel between these
415 compartments. Noteworthy, the initial phase of the Tg-induced Ca^{2+} release out of the ER
416 did not appear modified by TPEN, as if it was mediated by a Zn^{2+}-insensitive Ca^{2+}
417 channel(s)/transporter, contrasting with the abrogation of Ach-induced ER emptying from
418 the outset. Remarkably, independently of Zn^{2+} chelators, emptying of Ca^{2+} ER was

419 modified in a genetic model of Zn^{2+}-deficient oocytes lacking two TRP channels,
420 confirming the impact of Zn^{2+} on Ca^{2+} release. It is worth noting that TPEN did not reduce
421 but maintained or increased the mass of IP_3R1, which might result in the inhibition of
422 Zn^{2+}-dependent ubiquitin ligase Ubc7 by the Zn-deficient conditions (Webster et al.,
423 2003). We cannot rule out that these conditions may undermine other conformational
424 changes required to trigger IP_3R1 degradation, thereby favoring the accumulation of
425 IP_3R1.

426 Despite accruing Zn^{2+} during oocyte maturation, fertilization witnesses a
427 necessary Zn^{2+} release into the external milieu, known as "Zn^{2+} sparks" (Converse and
428 Thomas, 2020; Kim et al., 2011; Mendoza et al., 2022; Que et al., 2019, 2015; Seeler et
429 al., 2021). This release of Zn^{2+} is a conserved event in fertilization across species and is
430 associated with several biological functions, including those related to fending off
431 polyspermy (Kim et al., 2011; Que et al., 2019; Wozniak et al., 2020). The concomitant
432 decrease in Zn^{2+} facilitates the resumption of the cell cycle and exit from the MII stage
433 (Kim et al., 2011). Congruent with this observation, artificial manipulation that maintains
434 high Zn^{2+} levels prevents egg activation (Kim et al., 2011), whereas lowering Zn^{2+} with
435 chelators leads to egg activation without Ca^{2+} mobilization (Suzuki et al., 2010b). As
436 posed by others, these results suggest that meiosis completion and the early stages of
437 fertilization unfold within a narrow window of permissible Zn^{2+} (Kim et al., 2011, 2010).
438 Here, we extend this concept and show that IP_3R1 function and the Ca^{2+} oscillations in
439 mouse eggs require this optimal level of labile Zn^{2+} because the Ca^{2+} responses
440 interrupted by TPEN-induced Zn^{2+}-insufficiency are rescued by restoring Zn^{2+} levels with
441 ZnPT. Furthermore, unopposed increases in Zn^{2+} by exposure to ZnPT abrogated
442 fertilization-initiated Ca^{2+} oscillations and prevented the expected egg activation events.
443 It is unclear how excess Zn^{2+} disturbs the function of IP_3R1. Nevertheless, IP_3R1s have
444 multiple cysteines whose oxidation enhances the receptor sensitivity to IP_3 (Joseph et al.,
445 2018), and it is possible that excessive Zn^{2+} aberrantly modifies them, disturbing IP_3R1
446 structure and function or, alternatively, preventing their oxidation and sensitization of the
447 receptor. Lastly, we cannot rule out that high Zn^{2+} levels directly inhibit the receptor's
448 channel. These results reveal a close association between the Zn^{2+} levels controlling
449 meiotic transitions and the Ca^{2+} release necessary for egg activation, placing the IP_3R1 at
450 the center of the crosstalk of these two divalent cations.

451 Abrupt Zn^{2+} changes have emerged as critical signals for meiotic and mitotic
452 transitions in oocytes, eggs, embryos, and somatic cells (Kim et al., 2011, 2010; Lo et al.,
453 2020). Fertilization relies on prototypical Ca^{2+} rises and oscillations, and Zn^{2+} sparks are
454 an egg activation event downstream of this Ca^{2+} release, establishing a functional

455 association between these two divalent cations that continues to grow (Kim et al., 2011).
456 Here, we show that, in addition, these cations actively crosstalk during fertilization and
457 that the fertilization-induced Ca^{2+} oscillations rely on optimized IP_3R1 function
458 underpinned by ideal Zn^{2+} levels set during oocyte maturation. Future studies should
459 explore if artificial alteration of Zn^{2+} levels can extend the fertile lifespan of eggs,
460 improve developmental competence, or develop methods of non-hormonal contraception.
461

462 **Materials and Methods**

463 **Key resources table**

Reagent type (species) or resource	Designation	Source or reference	Identifiers	Additional information
Genetic reagent (*Mus musculus*)	CD1	Charles River	022	
Genetic reagent (*Mus musculus*)	C57BL/6J	JAX	JAX: 000664	
Genetic reagent (*Mus musculus*)	*Trpm7*-floxed	A generous gift from Dr. Carmen P. Williams (NIEHS) (PMID: 30322909)		C57BL6/J and 129s4/SvJae mixed background
Genetic reagent (*Mus musculus*)	*Gdf9-cre*	JAX	JAX: 011062	
Genetic reagent (*Mus musculus*)	*Trpv3*$^{-/-}$	A generous gift from Dr H. Xu (PMID: 20403327)		C57BL/6J and 129/SvEv mixed background
Biological sample (mouse oocyte)	*Mus musculus*	this paper		Eggs at the metaphase of the second meiosis
Biological sample (mouse	*Mus musculus*	this paper		Matured sperm from

sperm)				cauda epididymis
Recombinant DNA reagent	pcDNA6-mouse *Plcz1-venus* (plasmid used as a template for mRNA synthesis)	Published in previous Fissore lab paper PMID: 34313315. Mouse *Plcz1* sequence was a generous gift from Dr. Kiyoko Fukami (PMID:18028898)		mouse *Plcz1* mRNA was fused with Venus and inserted in pcDNA6 vector
Recombinant DNA reagent	pcDNA6-CALR-D1ER-KDEL (plasmid used as a template for mRNA synthesis)	Published in previous Fissore lab paper PMID: 24101727. Original D1ER vector was a generous gift from Dr. Roger Y Tsien (PMID: 15585581)		FRET construct D1ER was inserted between ER-targeting sequence of calreticulin and KDEL ER retention signal in pcDNA6 vector
Recombinant DNA reagent	pcDNA6-human *ERp44-HA* (plasmid used as a template for mRNA synthesis)	This paper. Original human ERp44 sequence was a generous gift from Dr. Roberto Sitia (PMID: 11847130)		human *ERp44* mRNA fused with HA in pcDNA6/ Myc-His B vector
Antibody	Monoclonal HA (Mouse monoclonal)	Roche	11581816001	Dilution: 1:200
Antibody	Polyclonal IP_3R1 (Rabbit polyclonal)	(Parys et al., 1995)		Dilution: 1:1000
Antibody	Monoclonal α-tubulin	Sigma-Aldrich	T-9026	Dilution:

	(Mouse monoclonal)			1:1000
Antibody	Alexa Fluor 488 (goat anti mouse)	Invitrogen	Invitrogen: A32723	Dilution: 1:400
Commercial assay or kit	T7 mMESSAGE mMACHINE Kit	Invitrogen	Invitrogen: AM1344	Used for *in vitro* mRNA synthesis
Commercial assay or kit	Poly(A) Tailing Kit	Invitrogen	Invitrogen: AM1350	Used for poly (A) tailing of synthesized mRNA
Chemical compound, drug	Hyaluronidase from bovine testes	Sigma-Aldrich	H3506	
Chemical compound, drug	3-Isobutyl-1-methylxanthine (IBMX)	Sigma-Aldrich	I5879	
Chemical compound, drug	Polyvinylpyrrolidone (PVP) (average molecular weight: 360,000)	Sigma-Aldrich	PVP360	Used for mRNA microinjection and ICSI
Chemical compound, drug	N,N, N′,N′-Tetrakis (2-pyridylmethyl) ethylenediamine (TPEN)	Sigma-Aldrich	P4413	Prepared in DMSO and kept at –20 °C until use
Chemical compound, drug	Zinc Pyrithione (ZnPT)	Sigma-Aldrich	PHR1401	Prepared in DMSO and kept at –20 °C until use
Chemical compound, drug	Strontium chloride hexahydrate ($SrCl_2$)	Sigma-Aldrich	255521	Freshly dissolved in water on the day of experiment
Chemical compound, drug	Calcium chloride dihydrate ($CaCl_2$)	Sigma-Aldrich	C3881	Freshly dissolved in water on the day of experiment

Chemical compound, drug	Magnesium chloride hexahydrate ($MgCl_2$)	Sigma-Aldrich	M2393	Freshly dissolved in water on the day of experiment
Chemical compound, drug	Zinc sulfate monohydrate ($ZnSO_4$)	Acros Organics	389802500	Freshly dissolved in water on the day of experiment
Chemical compound, drug	Ethylenediaminetetraacetic acid sodium dihydrate (EDTA)	LabChem	LC137501	Prepared as 0.5M aqueous solution with pH 8.0 adjusted by NaOH
Chemical compound, drug	Diethylenetriaminepentaacetic acid (DTPA)	Sigma-Aldrich	D6518	
Chemical compound, drug	Tris (2-pyridylmethyl) amine (TPA)	Santa Cruz	sc-477037	
Chemical compound, drug	Dimethyl sulphoxide (DMSO)	Sigma-Aldrich	D8418	Used as a solvent
Chemical compound, drug	Acetylcholine chloride	Sigma-Aldrich	A6625	
Chemical compound, drug	Thimerosal	Sigma-Aldrich	T5125	Freshly dissolved in water on the day of experiment and kept on ice until use
Chemical compound, drug	Ionomycin calcium salt	Tocris	1704	Working concentration: 2.5

				µM
Chemical compound, drug	Thapsigargin	Calbiochem	#586500	Working concentration: 10 µM
Other	Pluronic F-127 (20% solution in DMSO) (Pluronic acid)	Invitrogen	P3000MP	
Other	Fura-2 AM	Invitrogen	F1221	Used at 1.25 µM in TL-HEPES containing 0.02% Pluronic acid
Other	FluoZin-3 AM	Invitrogen	F24195	Used at 1.25 µM in TL-HEPES containing 0.02% Pluronic acid
Other	Fluo-4 AM	Invitrogen	F14201	Used at 1.25 µM in TL-HEPES containing 0.02% Pluronic acid
Other	Rhod2-AM	Invitrogen	R1244	Used at 2.2 µM in TL-HEPES containing 0.02% Pluronic acid.
Other	ci-IP3/ PM	Tocris	6210	Dissolved in DMSO and kept at –20 °C. Before use, the stock was

				diluted with water to make a final concentration of 0.25 mM.
Other	Pme1	New England BioLabs	R0560S	Used to linearize pcDNA6 vectors for mRNA synthesis
Software, algorithm	Prism	GraphPad Software		Version 5.01

N,N,N′,N′-tetrakis (2-pyridinylmethyl)-1,2-ethylenediamine (TPEN) and Zinc pyrithione (ZnPT) were dissolved in dimethyl sulfoxide (DMSO) at 10 mM and stored at -20°C until use. $SrCl_2$, $CaCl_2$, $ZnSO_4$, and $MgCl_2$ were freshly dissolved with double-sterile water at 1M and diluted with the monitoring media just before use. Ethylenediaminetetraacetic acid (EDTA) and diethylenetriaminepentaacetic acid (DTPA) were reconstituted with double-sterile water at 0.5M and 10 mM, respectively, and the pH was adjusted to 8.0. Tris(2-pyridylmethyl) amine (TPA) was diluted in DMSO at 100 mM and stored at -20°C until use. Acetylcholine chloride and Thimerosal were dissolved in double-sterile water at 550 mM and 100 mM, respectively. Acetylcholine was stored at -20°C until use, whereas Thimerosal was made fresh in each experiment.

Mice

The University of Massachusetts Institutional Animal Care and Use Committee (IACUC) approved all animal experiments and protocols. *Trpm7*-floxed (*Trpm7*$^{fl/fl}$) *Gdf9-Cre* and *Trpv3*$^{-/-}$ mice were bred at our facility. *Trpm7*$^{fl/fl}$ mice were crossed with *Trpv3*$^{-/-}$ to generate *Trpm7*$^{fl/fl}$; *Trpv3*$^{-/-}$ mouse line. Female *Trpm7*$^{fl/fl}$; *Trpv3*$^{-/-}$ mice were crossed with *Trpm7*$^{fl/fl}$; *Trpv3*$^{-/-}$; *Gdf9-cre* male to generate females null for *Trpv3* and with oocyte-specific deletion for *Trpm7*. Ear clips from offspring were collected prior to weaning, and confirmation of genotype was performed after most experiments.

Egg Collection

All gamete handling procedures are as previously reported by us (Wakai and Fissore,

487 2019). MII eggs were collected from the ampulla of 6- to 8-week-old female mice.
488 Females were superovulated via intraperitoneal injections of 5 IU pregnant mare serum
489 gonadotropin (PMSG, Sigma, St. Louis, MO) and 5 IU human chorionic gonadotropin
490 (hCG, sigma) at 48hr. interval. Cumulus-oocyte-complexes (COCs) were obtained 13.5
491 hr. post-hCG injection by tearing the ampulla using forceps and needles in TL-HEPES
492 medium. COCs were treated with 0.26% (w/v) of hyaluronidase at room temperature (RT)
493 for 5 min to remove cumulus cells.
494
495 **Intracytoplasmic sperm injection (ICSI)**
496 ICSI was performed as previously reported by us (Kurokawa and Fissore, 2003) using
497 described setup and micromanipulators (Narishige, Japan). Sperm from C57BL/6 or CD1
498 male mice (7-12 weeks old) were collected from the cauda epididymis in TL-HEPES
499 medium, washed several times, heads separated from tails by sonication (XL2020; Heat
500 Systems Inc., USA) for 5 s at 4°C. The sperm lysate was washed in TL-HEPES and
501 diluted with 12% polyvinylpyrrolidone (PVP, MW = 360 kDa) to a final PVP
502 concentration of 6%. A piezo micropipette-driving unit was used to deliver the sperm into
503 the ooplasm (Primetech, Ibaraki, Japan); a few piezo-pulses were applied to puncture the
504 eggs' plasma membrane following penetration of the zona pellucida. After ICSI, eggs
505 were either used for Ca^{2+} monitoring or cultured in KSOM to evaluate activation and
506 development at 36.5°C in a humidified atmosphere containing 5% CO_2.
507
508 **Preparation and microinjection of mRNA**
509 pcDNA6-m*Plcζ-mEGFP*, pcDNA6-CALR-D1ER-KDEL, and pcDNA6-*humanERp44-*
510 *HA* were linearized with the restriction enzyme PmeI and *in vitro* transcribed using the
511 T7 mMESSAGE mMACHINE Kit following procedures previously used in our
512 laboratory (Ardestani et al., 2020). A poly(A) tail was added to the *in vitro* synthesized
513 RNA (mRNA) using Tailing Kit followed by quantification and dilution to 0.5 μg/μL in
514 nuclease-free water and stored at -80°C until use. Before microinjection, m*Plcζ*, D1ER,
515 and *ERp44* mRNA were diluted to 0.01, 1.0, and 0.5 μg/μL, respectively, in nuclease-free
516 water, heated at 95°C for 3 min followed by centrifugation at 13400×*g* for 10 min at 4°C.
517 Cytoplasm injection of mRNA was performed under microscopy equipped with
518 micromanipulators (Narishige, Japan). The zona pellucida and the plasma membrane of
519 MII eggs were penetrated by applying small pulses generated by the piezo
520 micromanipulator (Primetech, Ibaraki, Japan). The preparation of the injection pipette
521 was as for ICSI (Kurokawa and Fissore, 2003), but the diameter of the tip was ~1 μm.
522

523 **Ca^{2+} and Zn^{2+} imaging**

524 Before Ca^{2+} imaging, eggs were incubated in TL-HEPES containing 1.25 μM Fura2-AM,
525 1.25 μM FluoZin3-AM, or 2.2 μM Rhod2-AM and 0.02% Pluronic acid for 20 min at
526 room temperature and then washed. The fluorescent probe-loaded eggs were allowed to
527 attach to the bottom of the glass dish (Mat-Tek Corp., Ashland, MA). Eggs were
528 monitored simultaneously using an inverted microscope (Nikon, Melville, NY) outfitted
529 for fluorescence measurements. Fura-2 AM, FluoZin3-AM, and Rhod2-AM fluorescence
530 were excited with 340 nm and 380 nm, 480 nm, and 550 nm wavelengths, respectively,
531 every 20 sec, for different intervals according to the experimental design and as
532 previously performed in the laboratory. The illumination was provided by a 75-W Xenon
533 arc lamp and controlled by a filter wheel (Ludl Electronic Products Ltd., Hawthorne, NY).
534 The emitted light above 510 nm was collected by a cooled Photometrics SenSys CCD
535 camera (Roper Scientific, Tucson, AZ). Nikon Element software coordinated the filter
536 wheel and data acquisition. The acquired data were saved and analyzed using Microsoft
537 Excel and GraphPad using Prism software (Ardestani et al., 2020). For Figures 1A, 4A-
538 C, 5A, and 6H-I, values obtained from FluoZin3-AM, Fura2-AM, or Rhod2-AM
539 recordings were divided by the average of the first five recordings for each treatment that
540 was used as the F_0.

541 To estimate relative changes in Ca^{2+}-ER, emission ratio imaging of the D1ER (YFP/CFP)
542 was performed using a CFP excitation filter, dichroic beamsplitter, CFP and YFP emission
543 filters (Chroma technology, Rockingham, VT; ET436/20X, 89007bs, ET480/40m, and
544 ET535/30m). To measure Ca^{2+}-ER and cytosolic Ca^{2+} simultaneously, eggs that had been
545 injected with D1ER were loaded with Rhod-2AM, and CFP, YFP, and Rhod-2 intensities
546 were collected every 20 sec.

547

548 **Caged IP_3**

549 Caged-IP_3/PM (cIP_3) was reconstituted in DMSO and stored at -20°C until use. Before
550 injection, cIP_3 stock was diluted to 0.25 mM with water and microinjected as above. After
551 incubation in KSOM media at 37°C for 1-hr., the injected eggs were loaded with the
552 fluorophore, 1.25 μM Fluo4-AM, and 0.02% Pluronic acid and handled as above for Fura-
553 2 AM. The release of cIP_3 was accomplished by photolysis using 0.5 to 5-sec pulses at
554 360 nm wavelengths. Ca^{2+} imaging was as above, but Fluo4 was excited at 488 nm
555 wavelength and emitted light above 510 nm collected as above.

556

557 **Western blot analysis**

558 Cell lysates from 20-50 mouse eggs were prepared by adding 2X- Laemmli sample buffer.

559 Proteins were separated on 5% SDS-PAGE gels and transferred to PVDF membranes
560 (Millipore, Bedford, MA). After blocking with 5% fat-free milk + TBS, membranes were
561 probed with the rabbit polyclonal antibody specific to IP_3R1 (1:1000; a generous gift from
562 Dr. Jan Parys, Katholieke Universiteit, Leuven, Belgium; Parys et al., 1995). Goat anti-
563 rabbit antibody conjugated to horseradish peroxidase (HRP) was used as a secondary
564 antibody (1:5000; Goat anti-Rabbit IgG (H+L) Cross-Adsorbed Secondary Antibody,
565 HRP; Invitrogen, Waltham, Ma). For detection of chemiluminescence, membranes were
566 developed using ECL Prime (Sigma) and exposed for 1–3 min to maximum sensitivity
567 film (VWR, Radnor, PA). Broad-range pre-stained SDS–PAGE molecular weight
568 markers (Bio-Rad, Hercules, CA) were run in parallel to estimate the molecular weight
569 of the immunoreactive bands. The same membranes were stripped at 50°C for 30 min
570 (62.5 mM Tris, 2% SDS, and 100 mM 2-beta mercaptoethanol) and re-probed with anti-
571 α-tubulin monoclonal antibody (1:1000).
572
573 **Immunostaining and confocal microscopy**
574 Immunostaining was performed according to our previous study (Akizawa et al., 2021).
575 After incubation with or without TPEN, MII eggs were fixed with 4% (w/v)
576 paraformaldehyde in house-made phosphate-buffered saline (PBS) for 20 min at room
577 temperature and then permeabilized for 60 min with 0.2% (v/v) Triton X-100 in PBS.
578 Next, the eggs were blocked for 45 min with a blocking buffer containing 0.2% (w/v)
579 skim milk, 2% (v/v) fetal bovine serum, 1% (w/v) bovine serum albumin, 0.1% (v/v)
580 TritonX-100, 0.75% (w/v) glycine in PBS. Eggs were incubated overnight at 4°C with
581 mouse anti-HA antibody (1:200) diluted in blocking buffer. Eggs were washed in blocking
582 buffer 3X for 10 min, followed by incubation at room temperature for 30 min with a
583 secondary antibody, Alexa Fluor 488 goat anti-mouse IgG (H + L) (1:400) diluted in
584 blocking buffer. Fluorescence signals were visualized using a laser-scanning confocal
585 microscope (Nikon A1 Resonant Confocal with six-color TIRF) fitted with a 63×, 1.4 NA
586 oil-immersion objective lens.
587
588 **Statistical analysis**
589 Comparisons for statistical significance of experimental values between treatments and
590 experiments were performed in three or more experiments performed on different batches
591 of eggs in most studies. Given the number of eggs needed, WB studies were repeated
592 twice. Prism-GraphPad software was used to perform the statistical comparisons that
593 include unpaired Student's t-tests, Fisher's exact test, and One-way ANOVA followed by
594 Tukey's multiple comparisons, as applicable, and the production of graphs to display the

data. All data are presented as mean±s.d. Differences were considered significant at $P < 0.05$.

Acknowledgments

We thank Ms. Changli He for technical support and Dr. James Chambers for support with confocal microscopy support. We thank all members of the Fissore lab for useful discussions and suggestions. We thank Jan B. Parys, K.U. Leuven, Belgium, for initial discussions and advice.

Competing interests

The authors declare no competing or financial interests.

Additional information

Funding Sources

Funder	Grant reference number	Author
National Institute of Health	RO1 HD092499	Rafael A. Fissore
National Institute of Food and Agriculture	2021-06893	MG. Gervasi, R.A. Fissore, P.E. Visconti
Japan Society for the Promotion of Science Overseas Research Fellowship	Postdoctoral fellowship	Hiroki Akizawa
The funders had no role in study design, data collection and interpretation, or the decision to submit the work for publication.		

Author contributions

Hiroki Akizawa, Data curation, Formal analysis, Validation, Investigation, Visualization, Writing—original draft, Writing—review and editing; Emily Lopes, Data curation, Formal analysis, Validation; Rafael A Fissore, Conceptualization, Formal analysis, Supervision, Funding acquisition, Methodology, Writing—original draft, Project administration, Writing—review and editing

References

Abbott AL, Xu Z, Kopf GS, Ducibella T, Schultz RM. 1998. In vitro culture retards spontaneous activation of cell cycle progression and cortical granule exocytosis that normally occur in vivo unfertilized mouse eggs. *Biol Reprod* **59**:1515–1521. doi:10.1095/biolreprod59.6.1515

Ajduk A, Małagocki A, Maleszewski M. 2008. Cytoplasmic maturation of mammalian

623 oocytes: Development of a mechanism responsible for sperm-induced Ca2+
624 oscillations. *Reprod Biol* **8**:3–22. doi:10.1016/S1642-431X(12)60001-1
625 Akizawa H, Saito S, Kohri N, Furukawa E, Hayashi Y, Bai H, Nagano M, Yanagawa Y,
626 Tsukahara H, Takahashi M, Kagawa S, Kawahara-Miki R, Kobayashi H, Kono T,
627 Kawahara M. 2021. Deciphering two rounds of cell lineage segregations during
628 bovine preimplantation development. *FASEB J* **35**:1–14.
629 doi:10.1096/fj.202002762RR
630 Ardestani G, Mehregan A, Fleig A, Horgen FD, Carvacho I, Fissore RA. 2020. Divalent
631 cation influx and calcium homeostasis in germinal vesicle mouse oocytes. *Cell*
632 *Calcium* **87**:102181. doi:10.1016/j.ceca.2020.102181
633 Arslan P, Di Virgilio F, Beltrame M. 1985. Cytosolic Ca2+ homeostasis in Ehrlich and
634 Yoshida carcinomas. A new, membrane-permeant chelator of heavy metals reveals
635 that these ascites tumor cell lines have normal cytosolic free Ca2+. *J Biol Chem*
636 **260**:2719–2727. doi:10.1016/s0021-9258(18)89421-2
637 Barnett B, Kretshmar H, Hartman F. 1977. Structural Characterization of Bis (jV-
638 oxopyridine-2-thionato) zinc (II). *Inorg Chem* **16**:1834–1838.
639 Bernhardt ML, Kim AM, O'Halloran T V., Woodruff TK. 2011. Zinc requirement during
640 meiosis I-meiosis II transition in mouse oocytes is independent of the MOS-MAPK
641 pathway. *Biol Reprod* **84**:526–536. doi:10.1095/biolreprod.110.086488
642 Bernhardt ML, Kong BY, Kim AM, O'Halloran T V., Woodruff TK. 2012. A Zinc-
643 Dependent Mechanism Regulates Meiotic Progression in Mammalian Oocytes. *Biol*
644 *Reprod* **86**:1–10. doi:10.1095/biolreprod.111.097253
645 Bernhardt ML, Padilla-Banks E, Stein P, Zhang Y, Williams CJ. 2017. Store-operated
646 Ca2+ entry is not required for fertilization-induced Ca2+ signaling in mouse eggs.
647 *Cell Calcium* **65**:63–72. doi:10.1016/j.ceca.2017.02.004
648 Berridge MJ. 2016. The inositol trisphosphate/calcium signaling pathway in health and
649 disease. *Physiol Rev* **96**:1261–1296. doi:10.1152/physrev.00006.2016
650 Bhanumathy C, Da Fonseca PCA, Morris EP, Joseph SK. 2012. Identification of
651 functionally critical residues in the channel domain of inositol trisphosphate
652 receptors. *J Biol Chem* **287**:43674–43684. doi:10.1074/jbc.M112.415786
653 Bootman MD, Taylor CW, Berridge MJ. 1992. The thiol reagent, thimerosal, evokes
654 Ca2+ spikes in HeLa cells by sensitizing the inositol 1,4,5-trisphosphate receptor. *J*
655 *Biol Chem* **267**:25113–25119. doi:10.1016/s0021-9258(19)74013-7
656 Brind S, Swann K, Carroll J. 2000. Inositol 1,4,5-trisphosphate receptors are
657 downregulated in mouse oocytes in response to sperm or adenophostin A but not to
658 increases in intracellular Ca2+ or egg activation. *Dev Biol* **223**:251–265.

659 doi:10.1006/dbio.2000.9728
660 Broun ER, Greist A, Tricot G, Hoffman R. 1990. Excessive Zinc Ingestion: A Reversible
661 Cause of Sideroblastic Anemia and Bone Marrow Depression. *JAMA J Am Med*
662 *Assoc* **264**:1441–1443. doi:10.1001/jama.1990.03450110087033
663 Carraway RE, Dobner PR. 2012. Zinc pyrithione induces ERK- and PKC-dependent
664 necrosis distinct from TPEN-induced apoptosis in prostate cancer cells. *Biochim*
665 *Biophys Acta - Mol Cell Res* **1823**:544–557. doi:10.1016/j.bbamcr.2011.09.013
666 Carvacho I, Ardestani G, Lee HC, McGarvey K, Fissore RA, Lykke-Hartmann K. 2016.
667 TRPM7-like channels are functionally expressed in oocytes and modulate post-
668 fertilization embryo development in mouse. *Sci Rep* **6**:1–12. doi:10.1038/srep34236
669 Carvacho I, Lee HC, Fissore RA, Clapham DE. 2013. TRPV3 Channels mediate
670 strontium-induced mouse-egg activation. *Cell Rep* **5**:1375–1386.
671 doi:10.1016/j.celrep.2013.11.007
672 Converse A, Thomas P. 2020. The zinc transporter ZIP9 (Slc39a9) regulates zinc
673 dynamics essential to egg activation in zebrafish. *Sci Rep* **10**:1–14.
674 doi:10.1038/s41598-020-72515-4
675 Deguchi R, Shirakawa H, Oda S, Mohri T, Miyazaki S. 2000. Spatiotemporal analysis of
676 Ca2+ waves in relation to the sperm entry site and animal-vegetal axis during Ca2+
677 oscillations in fertilized mouse eggs. *Dev Biol* **218**:299–313.
678 doi:10.1006/dbio.1999.9573
679 des Georges A, Clarke OB, Zalk R, Yuan Q, Condon KJ, Grassucci RA, Hendrickson
680 WA, Marks AR, Frank J. 2016. Structural Basis for Gating and Activation of RyR1.
681 *Cell* **167**:145-157.e17. doi:10.1016/j.cell.2016.08.075
682 Ducibella T, Huneau D, Angelichio E, Xu Z, Schultz RM, Kopf GS, Fissore R, Madoux
683 S, Ozil J-P. 2002. Egg-to-Embryo Transition Is Driven by Differential Responses to
684 Ca2+ Oscillation Number. *Dev Biol* **250**:280–291. doi:10.1006/dbio.2002.0788
685 Dupont G, McGuinness OM, Johnson MH, Berridge MJ, Borgese F. 1996. Phospholipase
686 C in mouse oocytes: Characterization of β and γ isoforms and their possible
687 involvement in sperm-induced Ca2+ spiking. *Biochem J* **316**:583–591.
688 doi:10.1042/bj3160583
689 Eppig JJ. 1996. Coordination of nuclear and cytoplasmic oocyte maturation in eutherian
690 mammals. *Reprod Fertil Dev* **8**:485–489. doi:10.1071/RD9960485
691 Evellin S, Nolte J, Tysack K, Dorp F Vom, Thiel M, Oude Weernink PA, Jakobs KH,
692 Webb EJ, Lomasney JW, Schmidt M. 2002. Stimulation of phospholipase C-ε by
693 the M3 muscarinic acetylcholine receptor mediated by cyclic AMP and the GTPase
694 Rap2B. *J Biol Chem* **277**:16805–16813. doi:10.1074/jbc.M112024200

Fan G, Baker ML, Wang Z, Baker MR, Sinyagovskiy PA, Chiu W, Ludtke SJ, Serysheva II. 2015. Gating machinery of InsP3R channels revealed by electron cryomicroscopy. *Nature* **527**:336–341. doi:10.1038/nature15249

Fan G, Baker MR, Terry LE, Arige V, Chen M, Seryshev AB, Baker ML, Ludtke SJ, Yule DI, Serysheva II. 2022. Conformational motions and ligand-binding underlying gating and regulation in IP3R channel. *Nat Commun* **13**:1–15. doi:10.1038/s41467-022-34574-1

Fissore RA, Longo FJ, Anderson E, Parys JB, Ducibella T. 1999. Differential distribution of inositol trisphosphate receptor isoforms in mouse oocytes. *Biol Reprod* **60**:49–57. doi:10.1095/biolreprod60.1.49

Fujiwara T, Nakada K, Shirakawa H, Shunichi M. 1993. Development of inositol trisphosphate-induced calcium release mechanism during maturation of hamster oocytes. *Dev Biol*.

Gee KR, Zhou ZL, Qian WJ, Kennedy R. 2002. Detection and imaging of zinc secretion from pancreatic, β-cells using a new fluorescent zinc indicator. *J Am Chem Soc* **124**:776–778. doi:10.1021/ja011774y

Hajnóczky G, Thomas AP. 1997. Minimal requirements for calcium oscillations driven by the IP3 receptor. *EMBO J* **16**:3533–3543. doi:10.1093/emboj/16.12.3533

Hamada K, Terauchi A, Mikoshiba K. 2003. Three-dimensional Rearrangements within Inositol 1,4,5-Trisphosphate Receptor by Calcium. *J Biol Chem* **278**:52881–52889. doi:10.1074/jbc.M309743200

Hara T, Yoshigai E, Ohashi T, Fukada T. 2022. Zinc transporters as potential therapeutic targets: An updated review. *J Pharmacol Sci* **148**:221–228. doi:10.1016/j.jphs.2021.11.007

Heim A, Tischer T, Mayer TU. 2018. Calcineurin promotes APC/C activation at meiotic exit by acting on both XErp1 and Cdc20. *EMBO Rep* **19**:1–10. doi:10.15252/embr.201846433

Higo T, Hattori M, Nakamura T, Natsume T, Michikawa T, Mikoshiba K. 2005. Subtype-specific and ER lumenal environment-dependent regulation of inositol 1,4,5-trisphosphate receptor type 1 by ERp44. *Cell* **120**:85–98. doi:10.1016/j.cell.2004.11.048

Iino M. 1990. Biphasic Ca2+ dependence of inositol 1,4,5-trisphosphate-induced Ca release in smooth muscle cells of the guinea pig taenia caeci. *J Gen Physiol* **95**:1103–1122. doi:10.1085/jgp.95.6.1103

Jean T, Klee CB. 1986. Calcium modulation of inositol 1,4,5-trisphosphate-induced calcium release from neuroblastoma x glioma hybrid (NG108-15) microsomes. *J*

731 *Biol Chem* **261**:16414–16420. doi:10.1016/s0021-9258(18)66582-2
732 Jellerette T, He CL, Wu H, Parys JB, Fissore RA. 2000. Down-regulation of the Inositol
733 1,4,5-Triphosphate Receptor in Mouse Eggs Following Fertilization or
734 Parthenogenetic Activation. *Dev Biol* **223**:238–250. doi:10.1006/dbio.2000.9675
735 Jellerette T, Kurokawa M, Lee B, Malcuit C, Yoon SY, Smyth J, Vermassen E, De Smedt
736 H, Parys JB, Fissore RA. 2004. Cell cycle-coupled [Ca2+]i oscillations in mouse
737 zygotes and function of the inositol 1,4,5-trisphosphate receptor-1. *Dev Biol* **274**:94–
738 109. doi:10.1016/j.ydbio.2004.06.020
739 Joseph SK, Young MP, Alzayady K, Yule DI, Ali M, Booth DM, Hajnóczky G. 2018.
740 Redox regulation of type-I inositol trisphosphate receptors in intact mammalian cells.
741 *J Biol Chem* **293**:17464–17476. doi:10.1074/jbc.RA118.005624
742 Kang D, Park JY, Han J, Bae IH, Yoon SY, Kang SS, Choi WS, Hong SG. 2003.
743 Acetylcholine induces Ca2+ oscillations via m3/m4 muscarinic receptors in the
744 mouse oocyte. *Pflugers Arch Eur J Physiol* **447**:321–327. doi:10.1007/s00424-003-
745 1184-y
746 Kaur K, Gupta R, Saraf SA, Saraf SK. 2014. Zinc: The metal of life. *Compr Rev Food*
747 *Sci Food Saf* **13**:358–376. doi:10.1111/1541-4337.12067
748 Kim AM, Bernhardt ML, Kong BY, Ahn RW, Vogt S, Woodruff TK, O'Halloran T V.
749 2011. Zinc sparks are triggered by fertilization and facilitate cell cycle resumption
750 in mammalian eggs. *ACS Chem Biol* **6**:716–723. doi:10.1021/cb200084y
751 Kim AM, Vogt S, O'Halloran T V., Woodruff TK. 2010. Zinc availability regulates exit
752 from meiosis in maturing mammalian oocytes. *Nat Chem Biol* **6**:674–681.
753 doi:10.1038/nchembio.419
754 Kurokawa M, Fissore RA. 2003. ICSI-generated mouse zygotes exhibit altered calcium
755 oscillations, inositol 1,4,5-trisphosphate receptor-1 down-regulation, and embryo
756 development. *Mol Hum Reprod* **9**:523–533. doi:10.1093/molehr/gag072
757 Lawrence Y, Ozil JP, Swann K. 1998. The effects of a Ca2+ chelator and heavy-metal-
758 ion chelators upon Ca2+ oscillations and activation at fertilization in mouse eggs
759 suggest a role for repetitive Ca2+ increases. *Biochem J* **335**:335–342.
760 doi:10.1042/bj3350335
761 Lee B, Vermassen E, Yoon SY, Vanderheyden V, Ito J, Alfandari D, De Smedt H, Parys
762 JB, Fissore RA. 2006. Phosphorylation of IP3R1 and the regulation of [Ca2+]i
763 responses at fertilization: A role for the MAP kinase pathway. *Development*
764 **133**:4355–4365. doi:10.1242/dev.02624
765 Lemos FO, Bultynck G, Parys JB. 2021. A comprehensive overview of the complex world
766 of the endo- and sarcoplasmic reticulum Ca2+-leak channels. *Biochim Biophys Acta*

767 - *Mol Cell Res* **1868**:119020. doi:10.1016/j.bbamcr.2021.119020
768 Liu M. 2011. The biology and dynamics of mammalian cortical granules. *Reprod Biol*
769 *Endocrinol* **9**:1–17. doi:10.1186/1477-7827-9-149
770 Lo MN, Damon LJ, Tay JW, Jia S, Palmer AE. 2020. Single cell analysis reveals multiple
771 requirements for zinc in the mammalian cell cycle. *Elife* **9**:1–24.
772 doi:10.7554/eLife.51107
773 Lorca T, Cruzalegui FH, Fesquet D, Cavadore J, Méry J, Means A, Marcel D. 1993.
774 Calmodulin-dependent protein kinase II mediates inactivation of MPF and CSF upon
775 fertilization of Xenopus eggs. *Nature* **366**:270–273.
776 Maret W, Li Y. 2009. Coordination dynamics of zinc in proteins. *Chem Rev* **109**:4682–
777 4707. doi:10.1021/cr800556u
778 Matsu-ura T, Shirakawa H, Suzuki KGN, Miyamoto A, Sugiura K, Michikawa T, Kusumi
779 A, Mikoshiba K. 2019. Dual-FRET imaging of IP 3 and Ca 2+ revealed Ca 2+ -
780 induced IP 3 production maintains long lasting Ca 2+ oscillations in fertilized mouse
781 eggs. *Sci Rep* **9**:1–11. doi:10.1038/s41598-019-40931-w
782 Mendivil-Perez M, Velez-Pardo C, Jimenez-Del-Rio M. 2012. TPEN induces apoptosis
783 independently of zinc chelator activity in a model of acute lymphoblastic leukemia
784 and Ex vivo acute leukemia cells through oxidative stress and mitochondria caspase-
785 3- and AIF-dependent pathways. *Oxid Med Cell Longev* **2012**.
786 doi:10.1155/2012/313275
787 Mendoza AD, Sue A, Antipova O, Vogt S, Woodruff TK, Wignall SM, O'halloran T V.
788 2022. Dynamic zinc fluxes regulate meiotic progression in Caenorhabditis elegans.
789 *Biol Reprod* **107**:406–418. doi:10.1093/biolre/ioac064
790 Miao YL, Stein P, Jefferson WN, Padilla-Banks E, Williams CJ. 2012. Calcium influx-
791 mediated signaling is required for complete mouse egg activation. *Proc Natl Acad*
792 *Sci U S A* **109**:4169–4174. doi:10.1073/pnas.1112333109
793 Miyazaki S. 1988. Inositol 1,4,5-trisphosphate-induced calcium release and guanine
794 nucleotide-binding protein-mediated periodic calcium rises in golden hamster eggs.
795 *J Cell Biol* **106**:345–353.
796 Miyazaki S, Ito M. 2006. Calcium signals for egg activation in mammals. *J Pharmacol*
797 *Sci* **100**:545–552. doi:10.1254/jphs.CPJ06003X
798 Miyazaki SI, Hashimoto N, Yoshimoto Y, Kishimoto T, Igusa Y, Hiramoto Y. 1986.
799 Temporal and spatial dynamics of the periodic increase in intracellular free calcium
800 at fertilization of golden hamster eggs. *Dev Biol* **118**:259–267. doi:10.1016/0012-
801 1606(86)90093-X
802 Miyazaki SI, Yuzaki M, Nakada K, Shirakawa H, Nakanishi S, Nakade S, Mikoshiba K.

1992. Block of Ca2+ wave and Ca2+ oscillation by antibody to the inositol 1,4,5-trisphosphate receptor in fertilized hamster eggs. *Science (80-)* **257**:251–255. doi:10.1126/science.1321497

Nomikos M, Elgmati K, Theodoridou M, Calver BL, Nounesis G, Swann K, Lai FA. 2011. Phospholipase Cζ binding to PtdIns(4,5)P 2 requires the XY-linker region. *J Cell Sci* **124**:2582–2590. doi:10.1242/jcs.083485

Nomikos M, Sanders JR, Parthimos D, Buntwal L, Calver BL, Stamatiadis P, Smith A, Clue M, Sideratou Z, Swann K, Lai FA. 2015. Essential role of the EF-hand domain in targeting sperm phospholipase Cζ to membrane phosphatidylinositol 4,5-bisphosphate (PIP2). *J Biol Chem* **290**:29519–29530. doi:10.1074/jbc.M115.658443

Pace NJ, Weerapana E. 2014. A competitive chemical-proteomic platform to identify zinc-binding cysteines. *ACS Chem Biol* **9**:258–265. doi:10.1021/cb400622

Paknejad N, Hite RK. 2018. Structural basis for the regulation of inositol trisphosphate receptors by Ca2+ and IP3. *Nat Struct Mol Biol* **25**:660–668. doi:10.1038/s41594-018-0089-6

Palmer AE, Jin C, Reed JC, Tsien RY. 2004. Bcl-2-mediated alterations in endoplasmic reticulum Ca2+ analyzed with an improved genetically encoded fluorescent sensor. *Proc Natl Acad Sci U S A* **101**:17404–17409. doi:10.1073/pnas.0408030101

Parrington J, Brind S, De Smedt H, Gangeswaran R, Anthony Lai F, Wojcikiewicz R, Carroll J. 1998. Expression of inositol 1,4,5-trisphosphate receptors in mouse oocytes and early embryos: The type I isoform is upregulated in oocytes and downregulated after fertilization. *Dev Biol* **203**:451–461. doi:10.1006/dbio.1998.9071

Parys JB, De Smedt H, Missiaen L, Bootman MD, Sienaert I, Casteels R. 1995. Rat basophiliv leukemia cells as model system for inositol 1,4,5-trisphosphate receptor IV, a receptor of the type II family: functional comparison and immunological detection. *Cell Calcium* **17**:239–249. doi:10.1016/0143-4160(95)90070-5

Perreault SD, Barbee RR, Slott VL. 1988. Importance of glutathione in the acquisition and maintenance of sperm nuclear decondensing activity in maturing hamster oocytes. *Dev Biol* **125**:181–186. doi:10.1016/0012-1606(88)90070-X

Qin Y, Dittmer PJ, Park JG, Jansen KB, Palmer AE. 2011. Measuring steady-state and dynamic endoplasmic reticulum and Golgi Zn 2+ with genetically encoded sensors. *Proc Natl Acad Sci U S A* **108**:7351–7356. doi:10.1073/pnas.1015686108

Que EL, Bleher R, Duncan FE, Kong BY, Gleber SC, Vogt S, Chen S, Garwin SA, Bayer AR, Dravid VP, Woodruff TK, O'Halloran T V. 2015. Quantitative mapping of zinc fluxes in the mammalian egg reveals the origin of fertilization-induced zinc sparks.

Nat Chem **7**:130–139. doi:10.1038/nchem.2133

Que EL, Duncan FE, Lee HC, Hornick JE, Vogt S, Fissore RA, O'Halloran T V., Woodruff TK. 2019. Bovine eggs release zinc in response to parthenogenetic and sperm-induced egg activation. *Theriogenology* **127**:41–48. doi:10.1016/j.theriogenology.2018.12.031

Richardson A, Taylor CW. 1993. Effects of Ca2+ chelators on purified inositol 1,4,5-trisphosphate (InsP3) receptors and InsP3-stimulated Ca2+ mobilization. *J Biol Chem* **268**:11528–11533. doi:10.1016/s0021-9258(19)50232-0

Ridgway EB, Gilkey JC, Jaffe LF. 1977. Free calcium increases explosively in activating medaka eggs. *Proc Natl Acad Sci U S A* **74**:623–627. doi:10.1073/pnas.74.2.623

Robinson MA. 1964. Complexes of 1-hydroxy 2-pyridinethione. *J Inorg Nucl Chem* **26**:1277–1281. doi:10.1016/0022-1902(64)80210-4

Sanders JR, Ashley B, Moon A, Woolley TE, Swann K. 2018. PLCζ induced Ca2+ oscillations in mouse eggs involve a positive feedback cycle of Ca2+ induced InsP3 formation from cytoplasmic PIP2. *Front Cell Dev Biol* **6**:1–14. doi:10.3389/fcell.2018.00036

Saunders CM, Larman MG, Parrington J, Cox LJ, Royse J, Blayney LM, Swann K, Lai FA. 2002. PLC zeta: a sperm-specific trigger of Ca(2+) oscillations in eggs and embryo development. *Development* **129**:3533–44.

Schultz RM, Kopf GS. 1995. Molecular Basis of Mammalian Egg Activation. *Curr Top Dev Biol* **30**:21–62. doi:10.1007/978-3-642-83139-3_7

Seeler JF, Sharma A, Zaluzec NJ, Bleher R, Lai B, Schultz EG, Hoffman BM, LaBonne C, Woodruff TK, O'Halloran T V. 2021. Metal ion fluxes controlling amphibian fertilization. *Nat Chem* **13**:683–691. doi:10.1038/s41557-021-00705-2

Shoji S, Muto Y, Ikeda M, He F, Tsuda K, Ohsawa N, Akasaka R, Terada T, Wakiyama M, Shirouzu M, Yokoyama S. 2014. The zinc-binding region (ZBR) fragment of Emi2 can inhibit APC/C by targeting its association with the coactivator Cdc20 and UBE2C-mediated ubiquitylation. *FEBS Open Bio* **4**:689–703. doi:10.1016/j.fob.2014.06.010

Shoji S, Yoshida N, Amanai M, Ohgishi M, Fukui T, Fujimoto S, Nakano Y, Kajikawa E, Perry ACF. 2006. Mammalian Emi2 mediates cytostatic arrest and transduces the signal for meiotic exit via Cdc20. *EMBO J* **25**:834–845. doi:10.1038/sj.emboj.7600953

Sienaert I, Missiaen L, De Smedt H, Parys JB, Sipma H, Casteels R. 1997. Molecular and functional evidence for multiple Ca2+-binding domains in the type 1 inositol 1,4,5-trisphosphate receptor. *J Biol Chem* **272**:25899–25906.

875 doi:10.1074/jbc.272.41.25899
876 Sikora J, Ouagazzal AM. 2021. Synaptic zinc: An emerging player in Parkinson's disease.
877 *Int J Mol Sci* **22**:1–16. doi:10.3390/ijms22094724
878 Sipma H, De Smet P, Sienaert I, Vanlingen S, Missiaen L, Parys JB, De Smedt H. 1999.
879 Modulation of inositol 1,4,5-trisphosphate binding to the recombinant ligand-
880 binding site of the type-1 inositol 1,4,5-trisphosphate receptor by Ca2+ and
881 calmodulin. *J Biol Chem* **274**:12157–12162. doi:10.1074/jbc.274.17.12157
882 Snitsarev VA, McNulty TJ, Taylor CW. 1996. Endogenous heavy metal ions perturb fura-
883 2 measurements of basal and hormone-evoked Ca2+ signals. *Biophys J* **71**:1048–
884 1056. doi:10.1016/S0006-3495(96)79305-0
885 Stein P, Savy V, Williams AM, Williams CJ. 2020. Modulators of calcium signalling at
886 fertilization. *Open Biol* **10**. doi:10.1098/rsob.200118
887 Stricker SA. 1999. Comparative biology of calcium signaling during fertilization and egg
888 activation in animals. *Dev Biol* **211**:157–176. doi:10.1006/dbio.1999.9340
889 Suzuki T, Suzuki E, Yoshida N, Kubo A, Li H, Okuda E, Amanai M, Perry ACF. 2010a.
890 Mouse Emi2 as a distinctive regulatory hub in second meiotic metaphase.
891 *Development* **137**:3281–3291. doi:10.1242/dev.052480
892 Suzuki T, Yoshida N, Suzuki E, Okuda E, Perry ACF. 2010b. Full-term mouse
893 development by abolishing Zn2+-dependent metaphase II arrest without Ca2+
894 release. *Development* **137**:2659–2669. doi:10.1242/dev.049791
895 Swann K, Parrington J. 1999. Mechanism of Ca2+ release at fertilization in mammals. *J*
896 *Exp Zool* **285**:267–275. doi:10.1002/(SICI)1097-010X(19991015)285:3<267::AID-
897 JEZ10>3.0.CO;2-P
898 Taylor CW, Tovey SC. 2010. IP3 Receptors: Toward Understanding Their Activation.
899 *Cold Spring Harb Perspect Biol* **2**:1–23.
900 Thastrup O, Cullen PJ, Drobak BK, Hanley MR, Dawson AP. 1990. Thapsigargin, a
901 tumor promoter, discharges intracellular Ca2+ stores by specific inhibition of the
902 endoplasmic reticulum Ca2+-ATPase. *Proc Natl Acad Sci U S A* **87**:2466–2470.
903 doi:10.1073/pnas.87.7.2466
904 Toeplitz BK, Cohen AI, Funke PT, Parker WL, Gougoutas JZ. 1979. Structure of
905 Ionomycin—A Novel Diacidic Polyether Antibiotic Having High Affinity for
906 Calcium Ions. *J Am Chem Soc* **101**:3344–3353. doi:10.1021/ja00506a035
907 Tokuhiro K, Dean J. 2018. Glycan-Independent Gamete Recognition Triggers Egg Zinc
908 Sparks and ZP2 Cleavage to Prevent Polyspermy. *Dev Cell* **46**:627-640.e5.
909 doi:10.1016/j.devcel.2018.07.020
910 Uchida K, Miyauchi H, Furuichi T, Michikawa T, Mikoshiba K. 2003. Critical regions

for activation gating of the inositol 1,4,5-trisphosphate receptor. *J Biol Chem* **278**:16551–16560. doi:10.1074/jbc.M300646200

Wakai T, Fissore RA. 2019. Constitutive IP3R1-mediated Ca2+ release reduces Ca2+ store content and stimulates mitochondrial metabolism in mouse GV oocytes. *J Cell Sci* **132**. doi:10.1242/jcs.225441

Wakai T, Fissore RA. 2013. Ca2+ homeostasis and regulation of ER Ca2+ in mammalian oocytes/eggs. *Cell Calcium* **53**:63–67. doi:10.1016/j.ceca.2012.11.010

Wakai T, Harada Y, Miyado K, Kono T. 2014. Mitochondrial dynamics controlled by mitofusins define organelle positioning and movement during mouse oocyte maturation. *Mol Hum Reprod* **20**:1090–1100. doi:10.1093/molehr/gau064

Wakai T, Mehregan A, Fissore RA. 2019. Ca2+ signaling and homeostasis in mammalian oocytes and eggs. *Cold Spring Harb Perspect Biol* **11**. doi:10.1101/cshperspect.a035162

Wakai T, Vanderheyden V, Yoon SY, Cheon B, Zhang N, Parys JB, Fissore RA. 2012. Regulation of inositol 1,4,5-trisphosphate receptor function during mouse oocyte maturation. *J Cell Physiol* **227**:705–717. doi:10.1002/jcp.22778

Wakai T, Zhang N, Vangheluwe P, Fissore RA. 2013. Regulation of endoplasmic reticulum Ca2+ oscillations in mammalian eggs. *J Cell Sci* **126**:5714–5724. doi:10.1242/jcs.136549

Walker JW, Somlyo A V., Goldman YE, Somlyo AP, Trentham DR. 1987. Kinetics of smooth and skeletal muscle activation by laser pulse photolysis of caged inositol 1,4,5-trisphosphate. *Nature* **327**:249–252.

Watanabe S, Amagai Y, Sannino S, Tempio T, Anelli T, Harayama M, Masui S, Sorrentino I, Yamada M, Sitia R, Inaba K. 2019. Zinc regulates ERp44-dependent protein quality control in the early secretory pathway. *Nat Commun* **10**:1–16. doi:10.1038/s41467-019-08429-1

Webster JM, Tiwari S, Weissman AM, Wojcikiewicz RJH. 2003. Inositol 1,4,5-trisphosphate receptor ubiquitination is mediated by mammalian Ubc7, a component of the endoplasmic reticulum-associated degradation pathway, and is inhibited by chelation of intracellular Zn2+. *J Biol Chem* **278**:38238–38246. doi:10.1074/jbc.M305600200

Woodier J, Rainbow RD, Stewart AJ, Pitt SJ. 2015. Intracellular zinc modulates cardiac ryanodine receptor-mediated calcium release. *J Biol Chem* **290**:17599–17610. doi:10.1074/jbc.M115.661280

Wozniak KL, Bainbridge RE, Summerville DW, Tembo M, Phelps WA, Sauer ML, Wisner BW, Czekalski ME, Pasumarthy S, Hanson ML, Linderman MB, Luu CH,

947 Boehm ME, Sanders SM, Buckley KM, Bain DJ, Nicotra ML, Lee MT, Carlson AE.
948 2020. Zinc protection of fertilized eggs is an ancient feature of sexual reproduction
949 in animals. *PLoS Biol* **18**:1–17. doi:10.1371/journal.pbio.3000811
950 Wu H, Smyth J, Luzzi V, Fukami K, Takenawa T, Black SL, Allbritton NL, Fissore RA.
951 2001. Sperm factor induces intracellular free calcium oscillations by stimulating the
952 phosphoinositide pathway. *Biol Reprod* **64**:1338–1349.
953 doi:10.1095/biolreprod64.5.1338
954 Wu L, Sweet T, Clapham DE. 2010. Current Progress in the Mammalian TRP Ion
955 Channel Family. *Pharmocol Rev* **62**:381–404.
956 doi:10.1124/pr.110.002725.Abbreviations
957 Xu Z, Williams CJ, Kopf GS, Schultz RM. 2003. Maturation-associated increase in IP3
958 receptor type 1: Role in conferring increased IP3 sensitivity and Ca2+ oscillatory
959 behavior in mouse eggs. *Dev Biol* **254**:163–171. doi:10.1016/S0012-
960 1606(02)00049-0
961 Yamasaki S, Sakata-Sogawa K, Hasegawa A, Suzuki T, Kabu K, Sato E, Kurosaki T,
962 Yamashita S, Tokunaga M, Nishida K, Hirano T. 2007. Zinc is a novel intracellular
963 second messenger. *J Cell Biol* **177**:637–645. doi:10.1083/jcb.200702081
964 Zhang N, Duncan FE, Que EL, O'Halloran T V., Woodruff TK. 2016. The fertilization-
965 induced zinc spark is a novel biomarker of mouse embryo quality and early
966 development. *Sci Rep* **6**:1–9. doi:10.1038/srep22772
967

968 **Table**

969 **Table 1. Addition of TPEN after ICSI does not prevent extrusion of the second polar**
970 **body but precludes pronuclear (PN) formation.**

Group*	No. of zygotes	2nd polar body (2.5h)	PN	
			4h	7h
Untreated	26	25 (96.1%)	23 (88.5%)	23 (88.5%)
TPEN (10μM)	27	24 (88.9%)	1 (3.7%)***	2 (7.4%)***

971 ***$P < 0.001$

972 *Data from three different replicates for each group.

973 **Figures Legends**

974 **Figure 1. TPEN-induced Zn^{2+} deficiency inhibits fertilization-initiated Ca^{2+}**
975 **oscillations in a dose-dependent manner.**

976 (**A**) (Left panel) Representative normalized Zn^{2+} recordings of MII eggs loaded with
977 FluoZin-3AM following the addition of increasing concentrations of TPEN (0 μM,
978 DMSO, black trace; 2.5 μM, sky blue; 5 μM, blue; 10 μM, navy). TPEN was directly
979 added to the monitoring media. (Right panel) Representative fluorescent images of MII
980 eggs loaded FluoZin-3AM supplemented with 0, 2.5, and 10 μM of TPEN. Scale bar: 10
981 μm. (**B-D**). (**B**) Representative Ca^{2+} oscillations following ICSI after the addition of 0, 5,
982 10, or 50 μM TPEN (arrowheads). Insets show representative traces for eggs that resumed
983 Ca^{2+} oscillations after TPEN. (**C**) As above, but following the addition of 100 μM EDTA,
984 100 or 500 μM DTPA (time of addition denoted by arrowheads). (**D**) Ca^{2+} oscillations
985 following ICSI after the addition of 50, 100, and 500 μM TPA (horizontal bars of
986 increasing thickness). (**E**) Representative bright field images of ICSI fertilized eggs 2.5,
987 4, and 7 h after sperm injection. Arrows and arrowheads denote the second polar body
988 and PN formation, respectively. Scale bar: 10 μm.

989

990 **Figure 2. TPEN dose-dependently inhibits Ca^{2+} oscillations in eggs triggered by a**
991 **broad-spectrum of agonists that stimulate the PI pathway or IP_3R1.**

992 (**A-D**) Representative Ca^{2+} responses induced by (**A**) m*Plcζ* mRNA microinjection (0.01
993 μg/μl, black traces), (**B**) strontium chloride (10 mM, green), (**C**) acetylcholine chloride
994 (50 μM, orange), and (**D**) thimerosal (25 μM, purple) in MII eggs. Increasing
995 concentrations of TPEN were added to the monitoring media (arrowheads above traces
996 denotes the time of adding). Insets in the upper row show representative traces of eggs
997 that stop oscillating despite others continuing to oscillate. (**E**) Each bar graph summarizes
998 the TPEN effect on Ca^{2+} oscillations at the selected concentrations for each of the agonists
999 in A-D. (**F**) Western blot showing the intensities of IP_3R1 and alpha-tubulin bands in MII
1000 eggs or in eggs injected with m*Plcζ* mRNA and incubated or not with TPEN above ($P <$
1001 0.01). Thirty eggs per lane in all cases. This experiment was repeated twice, and the mean
1002 relative intensity of each blot is shown in the bar graph below.

1003

1004 **Figure 3. TPEN inhibition of cIP_3-induced Ca^{2+} release is precluded by $ZnSO_4$**
1005 **supplementation before TPEN exposure.**

1006 (**A-G**) Representative Ca^{2+} responses in MII eggs triggered by the release of caged IP_3
1007 (cIP_3) induced by UV light pulses of increasing duration (arrows). (**A**) A representative
1008 control trace without TPEN, and (**B**) following the addition of 10 μM TPEN between the

1009 third and the fourth pulses. The broken line rectangle is magnified in the inset, farthest
1010 right side of the panel displaying the near immediate termination of an ongoing rise. (**C,**
1011 **D**) Recordings started in the presence of 10 μM TPEN but in (**D**) 100 μM $ZnSO_4$ was
1012 added between the second and the third pulses. (**E**) Recording started in the presence of
1013 100 μM $ZnSO_4$ followed by the addition of 10 μM TPEN between the third and the fourth
1014 pulses. (**F, G**) Recording started in the presence of 100 μM $MgSO_4$ (**F**) or 100 μM $CaCl_2$
1015 (**G**) and 10 μM TPEN added as above. Arrowheads above the different panels indicate
1016 the time of TPEN or divalent cation addition. (**H**) Bar graphs summarizing the number
1017 and percentages of eggs that responded to a given duration of UV pulses under each of
1018 the TPEN±divalent ions.
1019
1020 **Figure 4. Zn^{2+} depletion alters Ca^{2+} homeostasis and increases Ca^{2+} store content**
1021 **independent of IP_3R1 mass.**
1022 (**A, B**) Representative Ca^{2+} traces of MII eggs after the addition of Tg and Io in the
1023 presence or absence of TPEN. Blue trace recordings represent TPEN-treated eggs
1024 whereas gray traces represent control, untreated eggs. (**A**) Io was added to fresh MII
1025 eggs once Ca^{2+} returned to baseline after treatment with Tg. Comparisons of mean peak
1026 amplitudes after Tg and Io are shown in the bar graphs in the right panel ($P < 0.001$).
1027 (**B**) MII eggs were aged by 2h. incubation supplemented or not with TPEN followed by
1028 Io addition and Ca^{2+} monitoring ($P < 0.001$). (**C**) Western blot showing the intensities of
1029 IP_3R1 bands in MII eggs freshly collected, aged by 4h. incubation without TPEN, and
1030 with TPEN. Thirty eggs per lane in all cases. This experiment was repeated three times.
1031 (**D, E**) (Left panels) Representative traces of Ca^{2+} values in eggs loaded with the Ca^{2+}-
1032 sensitive dye Rhod-2 AM and the ER Ca^{2+}reporter, D1ER (1 μg/μl mRNA). TPEN was
1033 added into the media followed 10 min later by (**D**) 10 μM Tg and (**E**) 50 μM Ach.
1034 (Right panel) Bars represent the difference of FRET value between at the time of Tg/
1035 Ach addition and at 3 and 5 min later of the addition ($P < 0.05$). Experiments were
1036 repeated two different times for each treatment. Black and green traces represent
1037 cytosolic Ca^{2+} and Ca^{2+}-ER, respectively. Blue and black arrowheads indicate the time
1038 of addition of TPEN and Tg/ Ach, respectively. (**F**) Basal Zn^{2+} level comparison in WT
1039 (open bar) and *Trpv3*$^{-/-}$/*Trpm7*$^{-/-}$ (dKO, orange bar) MII eggs. Each plot represents the
1040 Fluozin3 measurement at 5 min after starting monitoring. (**G**) (Left panel)
1041 Representative Ca^{2+} traces of WT (black trace) and dKO (orange trace) MII eggs after
1042 adding Tg. Insets represent the magnified traces at the peak of Ca^{2+} spike from different
1043 sets of eggs. (Middle panel) Individual traces of WT and dKO eggs after Tg addition.
1044 Dashed circles represent the flection point in dKO traces. (Right panel) Comparisons of

1045 mean peak amplitudes after Tg and the time between Tg addition and the Ca^{2+} peak are
1046 shown in the bar graphs in the right panel ($P < 0.001$).
1047
1048 **Figure 5. Restoring Zn^{2+} levels with ZnPT rescues oscillations interrupted by TPEN-**
1049 **induced Zn^{2+} deficiency.**
1050 (**A**) Representative traces of Zn^{2+} in MII eggs following the addition of 0.01 to 0.1 μM
1051 concentrations of ZnPT. The broken rectangular area is amplified in the next panel to
1052 appreciate the subtle increase in basal Zn^{2+} caused by the addition of ZnPT. (**B, C**) m*Plcζ*
1053 mRNA (0.01 μg/μl)-induced oscillations followed by the addition of TPEN (black
1054 arrowhead) (**B**), or after the addition of TPEN followed by ZnPT (red arrowhead) (**C**). (**D,**
1055 **E**) Thimerosal (25 μM) induced oscillations using the same sequence of TPEN (**D**) and
1056 ZnPT (**E**), but higher concentrations of ZnPT were required to rescue Thimerosal-initiated
1057 oscillations (**E**). These experiments were repeated at least two different times.
1058
1059 **Figure 6. Excess Zn^{2+} hinders Ca^{2+} oscillations.**
1060 (**A-D**) ICSI-initiated Ca^{2+} response without (**A**) or following the addition of ZnPT (**B, C**)
1061 (the time of ZnPT addition and concentration are denoted above the tracing). (**E**, **F**)
1062 Representative Ca^{2+} responses induced by injection of 0.01 μg/μl m*Plcζ* mRNA in
1063 untreated eggs (**E**) or in eggs treated with 0.1 μM ZnPT followed by 10 μM TPEN first
1064 and then 50 μM (**F**). (**G**) cIP_3-induced Ca^{2+} release as expected when the UV pulses in
1065 the absence but not in the presence of 0.05 μM ZnPT (the time of addition is denoted by
1066 a bar above the tracing). (**H, I**) Representative traces of Ca^{2+} values in eggs loaded with
1067 the Ca^{2+}-sensitive dye Rhod-2 AM and the ER Ca^{2+}reporter, D1ER (1 μg/μl mRNA).
1068 Uninjected and 0.01 μg/μl m*Plcζ* mRNA-injected eggs were monitored. After initiation
1069 and establishment of the oscillations, 0.1 μM ZnPT was added into the media followed
1070 30 min later by 2.5 μM Io. Experiments were repeated two different times. Red and black
1071 arrowheads indicate the time of addition of ZnPT and Io, respectively.
1072
1073 **Figure 7. Schematic of proposed regulation of IP_3R1 function by Zn^{2+} in eggs and**
1074 **fertilized zygotes.**
1075 In MII eggs, left panel, IP_3R1s are in a Ca^{2+}-release permissive state with optimal levels
1076 of cytoplasmic Ca^{2+} and Zn^{2+} and maximum ER content, but Ca^{2+} is maintained at resting
1077 levels by the combined actions of pumps, ER Ca^{2+} leak, and reduced influx. Once
1078 fertilization takes place, left center panel, robust IP_3 production induced by the sperm-
1079 borne PLCζ leads to Ca^{2+} release through ligand-induced gating of IP_3R1. Continuous IP_3
1080 production and refilling of the stores via Ca^{2+} influx ensure the persistence of the

oscillations. Zn^{2+} release occurs in association with first few Ca^{2+} rises and cortical granule exocytosis, Zn^{2+} sparks, lowering Zn^{2+} levels but not sufficiently to inhibit IP_3R1 function. Zn^{2+} deficiency caused by TPEN or other permeable Zn^{2+} chelators, right center panel, dose-dependently impairs IP_3R1 function and limits Ca^{2+} release. We propose this is accomplished by stripping the Zn^{2+} bound to the residues of the zinc-finger motif in the LNK domain of IP_3R1 that prevents the allosteric modulation of the gating process induced by IP_3 or other agonists. We propose that excess Zn^{2+}, right panel, also inhibits IP_3R1-mediate Ca^{2+} release, possibly by non-specific binding of thiol groups present in cysteine residues throughout the receptor (denoted by a ?). We submit that optimal Ca^{2+} oscillations in mouse eggs unfold in the presence of a permissive range of Zn^{2+} concentration.

1092 **Supplementary Figure Legends**

1093

1094 **Supplementary Figure 1. Cell-impermeable chelators effectively reduce Zn^{2+} levels**
1095 **in external media but do prevent initiation or continuation of Ca^{2+} oscillations.**
1096 (**A**) A representative trace of FluoZin3 fluorescence in replete monitoring media (TL-HEPES). The
1097 media was supplemented with cell-impermeable FluoZin-3, and after initiation of monitoring, the
1098 addition of EDTA (100 μM) occurred at the designated point (triangle). (**B**) The left black trace
1099 represents Ca^{2+} oscillations initiation by injection of *mPlcζ* mRNA (0.01 μg/μl). The oscillations were
1100 monitored in Ca^{2+} and Mg^{2+}-free media and in the presence of EDTA (110 μM) to chelate residual
1101 divalent cations derived from the water source or reagents used to make the media. The right red trace
1102 represents the initiation of oscillations as above, but after a period indicated by the black and green
1103 bars, Ca^{2+} and Mg^{2+} were sequentially added back.

1104

1105 **Supplementary Figure 2. Overexpression of ER accessory protein ERp44 did not**
1106 **change the Ca^{2+} responses initiated by m*Plcζ* mRNA microinjection, Actylcholine,**
1107 **or $SrCl_2$.**
1108 (**A**) Representative immunofluorescent images of MII eggs with overexpression of
1109 ERp44. At 5 hr. post microinjection, eggs were treated with 10 or 50 μM of TPEN and
1110 incubated for 1 hr, after which they were fixed and stained. An anti-HA antibody was
1111 used. Scale bar: 10 μm. (**B**) Representative Ca^{2+} responses induced by m*Plcζ* mRNA
1112 microinjection (0.01 μg/ μl-left column), $SrCl_2$ (10 mM-center column), and
1113 acetylcholine (50 μM-right column) in eggs with (top panels) or without (bottom panels)
1114 ERp44 overexpression.

1115

1116 **Supplementary Figure 3. Elevated Zn^{2+} impairs egg activation and the subsequent**
1117 **embryo development.**
1118 (**A**) MII eggs were incubated in TL-HEPES containing 0, 0.1, or 1.0 μM ZnPT at room
1119 temperature for 10 min and washed several times with fresh TL-HEPES and injected with
1120 m*Plcζ* mRNA. After it, eggs and zygotes were cultured in KSOM for 24h. PN formation
1121 and 2-cell development were checked at 7 and 24h post-microinjection. Bars represent
1122 the percentages of injected eggs that reached the PN and the 2-cell stage. Scale bar: 50
1123 μm. (**B**) MII eggs injected with m*Plcζ* mRNA were incubated in KSOM without ZnPT
1124 for an hr. and then incubated in KSOM with 0 or 0.1 μM ZnPT for 24h. The second polar
1125 body extrusion, PN formation, and 2-cell development were checked at 2.5-, 7- and 24h.
1126 post-microinjection. Bars represent the percentages of injected eggs that reached the PN
1127 and the 2-cell stage. Scale bar: 50 μm.

Figure 1.

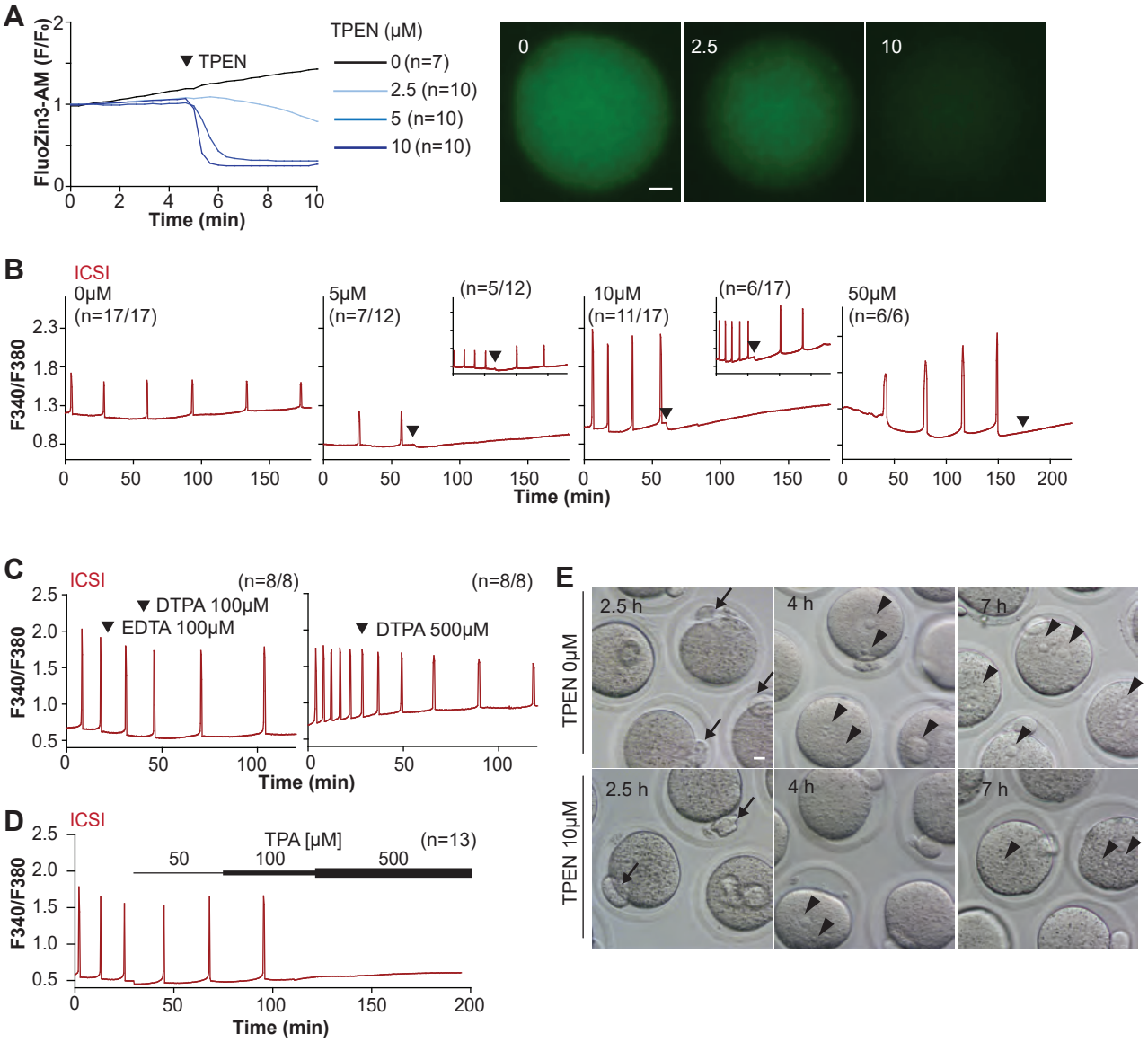
A
FluoZin3-AM (F/F0)
TPEN
TPEN (μM)
0 (n=7)
2.5 (n=10)
5 (n=10)
10 (n=10)
Time (min)
0
2.5
10
B
ICSI
0μM
(n=17/17)
5μM
(n=7/12)
(n=5/12)
10μM
(n=11/17)
(n=6/17)
50μM
(n=6/6)
F340/F380
Time (min)
C
ICSI
(n=8/8)
DTPA 100μM
EDTA 100μM
(n=8/8)
DTPA 500μM
F340/F380
Time (min)
D
ICSI
TPA [μM]
(n=13)
50
100
500
F340/F380
Time (min)
E
TPEN 0μM
TPEN 10μM
2.5 h
4 h
7 h

Figure 2.

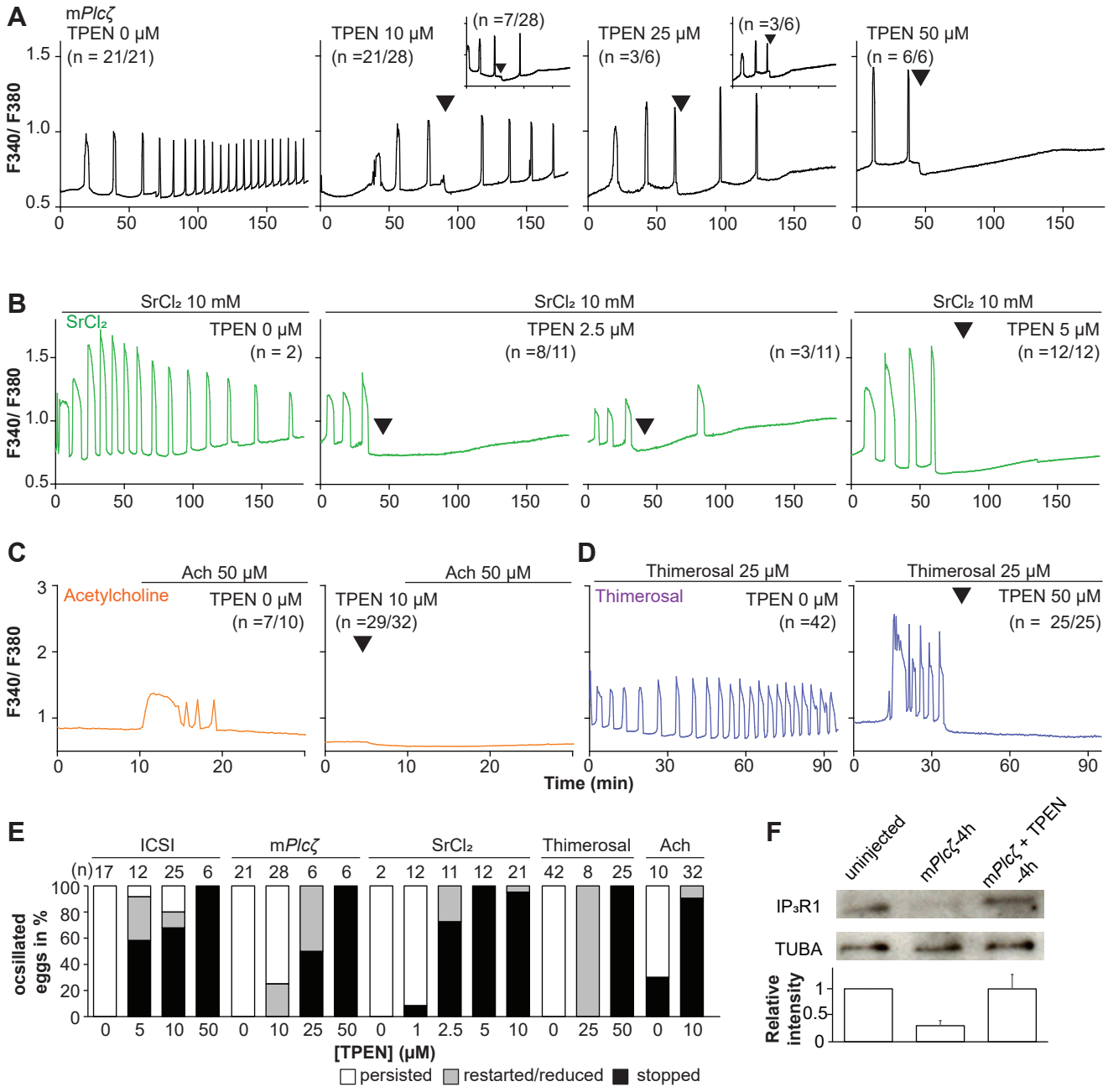
A
mPlcζ
TPEN 0 μM
(n = 21/21)
TPEN 10 μM
(n =21/28)
(n =7/28)
TPEN 25 μM
(n =3/6)
(n =3/6)
TPEN 50 μM
(n = 6/6)
F340/ F380
B
SrCl₂ 10 mM
SrCl₂
TPEN 0 μM
(n = 2)
TPEN 2.5 μM
(n =8/11)
(n =3/11)
TPEN 5 μM
(n =12/12)
C
Ach 50 μM
Acetylcholine
TPEN 0 μM
(n =7/10)
TPEN 10 μM
(n =29/32)
D
Thimerosal 25 μM
Thimerosal
TPEN 0 μM
(n =42)
TPEN 50 μM
(n = 25/25)
Time (min)
E
ICSI
mPlcζ
SrCl₂
Thimerosal
Ach
(n) 17 12 25 6 21 28 6 6 2 12 11 12 21 42 8 25 10 32
ocsillated eggs in %
[TPEN] (μM)
persisted
restarted/reduced
stopped
F
uninjected
mPlcζ-4h
mPlcζ + TPEN -4h
IP₃R1
TUBA
Relative intensity

Figure 3.

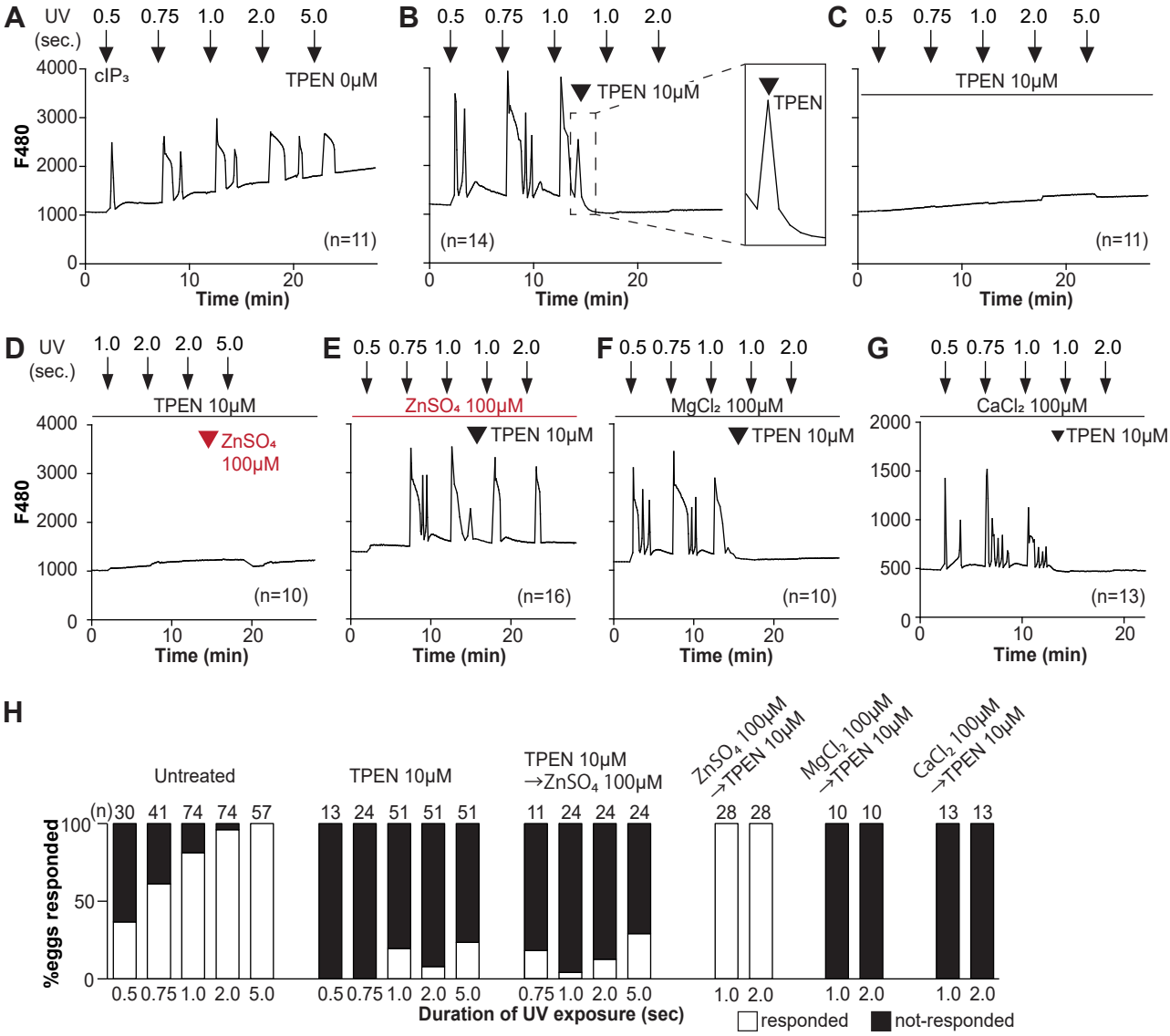
A
UV (sec.)
0.5 0.75 1.0 2.0 5.0
cIP₃
TPEN 0μM
F480
(n=11)
Time (min)
B
0.5 0.75 1.0 1.0 2.0
TPEN 10μM
TPEN
(n=14)
Time (min)
C
0.5 0.75 1.0 2.0 5.0
TPEN 10μM
(n=11)
Time (min)
D
UV (sec.)
1.0 2.0 2.0 5.0
TPEN 10μM
ZnSO₄ 100μM
F480
(n=10)
Time (min)
E
0.5 0.75 1.0 1.0 2.0
ZnSO₄ 100μM
TPEN 10μM
(n=16)
Time (min)
F
0.5 0.75 1.0 1.0 2.0
MgCl₂ 100μM
TPEN 10μM
(n=10)
Time (min)
G
0.5 0.75 1.0 1.0 2.0
CaCl₂ 100μM
TPEN 10μM
(n=13)
Time (min)
H
Untreated
TPEN 10μM
TPEN 10μM →ZnSO₄ 100μM
ZnSO₄ 100μM →TPEN 10μM
MgCl₂ 100μM →TPEN 10μM
CaCl₂ 100μM →TPEN 10μM
(n) 30 41 74 74 57
13 24 51 51 51
11 24 24 24
28 28
10 10
13 13
%eggs responded
0.5 0.75 1.0 2.0 5.0
0.5 0.75 1.0 2.0 5.0
0.75 1.0 2.0 5.0
1.0 2.0
1.0 2.0
1.0 2.0
Duration of UV exposure (sec)
responded
not-responded

Figure 4.

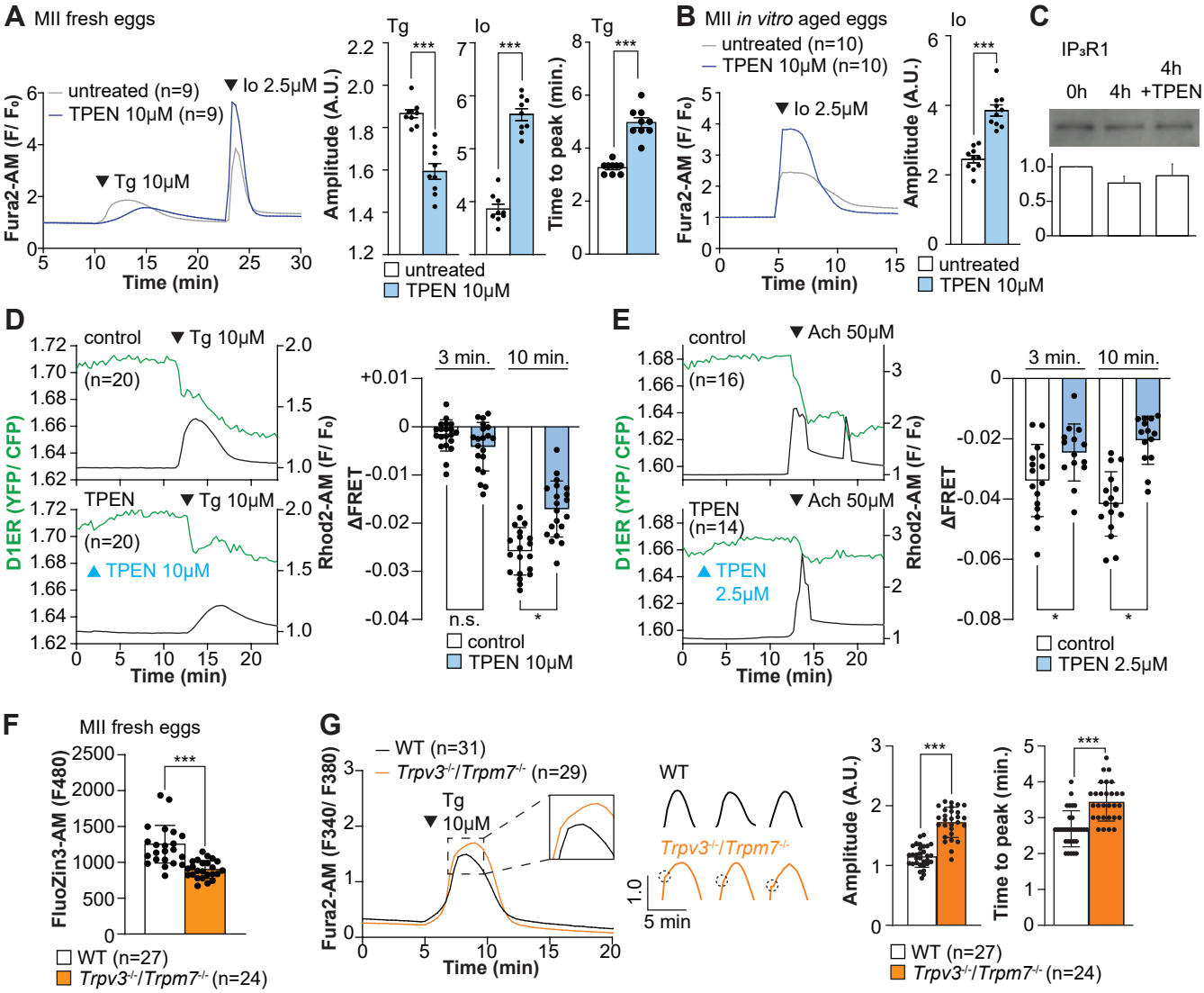
A MII fresh eggs
untreated (n=9)
TPEN 10μM (n=9)
Tg 10μM
Io 2.5μM
Fura2-AM (F/ F₀)
Time (min)
Tg
Io
Amplitude (A.U.)
Time to peak (min.)
untreated
TPEN 10μM
B MII in vitro aged eggs
untreated (n=10)
TPEN 10μM (n=10)
Io 2.5μM
C
IP₃R1
0h
4h
4h +TPEN
D
control
(n=20)
Tg 10μM
TPEN
(n=20)
TPEN 10μM
D1ER (YFP/ CFP)
Rhod2-AM (F/ F₀)
ΔFRET
3 min.
10 min.
n.s.
control
TPEN 10μM
E
control
(n=16)
Ach 50μM
TPEN
(n=14)
TPEN 2.5μM
TPEN 2.5μM
F MII fresh eggs
FluoZin3-AM (F480)
WT (n=27)
Trpv3-/-/Trpm7-/- (n=24)
G
WT (n=31)
Trpv3-/-/Trpm7-/- (n=29)
Tg 10μM
Fura2-AM (F340/ F380)
WT
Trpv3-/-/Trpm7-/-
1.0
5 min

Figure 5.

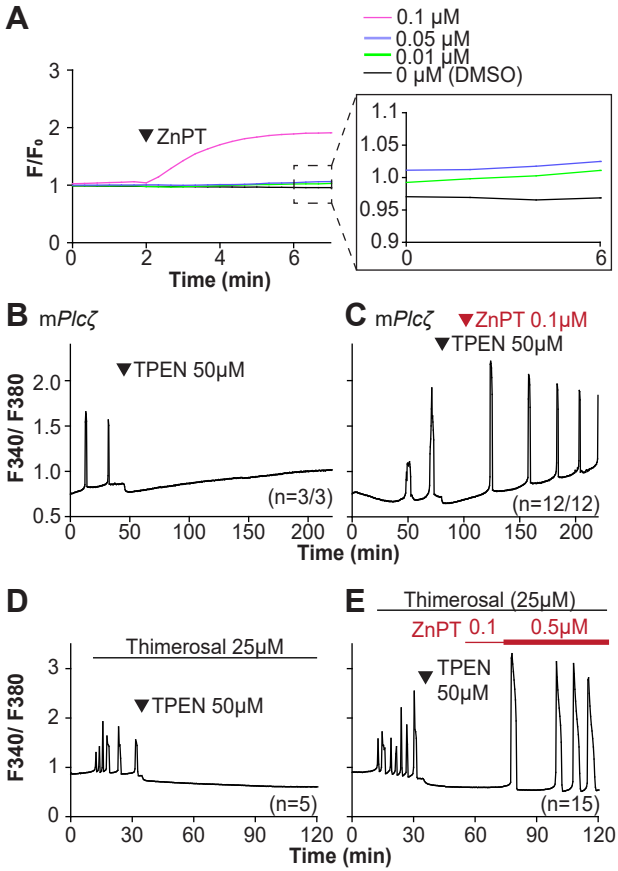
A
0.1 μM
0.05 μM
0.01 μM
0 μM (DMSO)
F/F0
ZnPT
Time (min)
B mPlcζ
TPEN 50μM
F340/ F380
(n=3/3)
Time (min)
C mPlcζ
ZnPT 0.1μM
TPEN 50μM
(n=12/12)
D
Thimerosal 25μM
TPEN 50μM
F340/ F380
(n=5)
Time (min)
E
Thimerosal (25μM)
ZnPT 0.1
0.5μM
TPEN 50μM
(n=15)

Figure6.

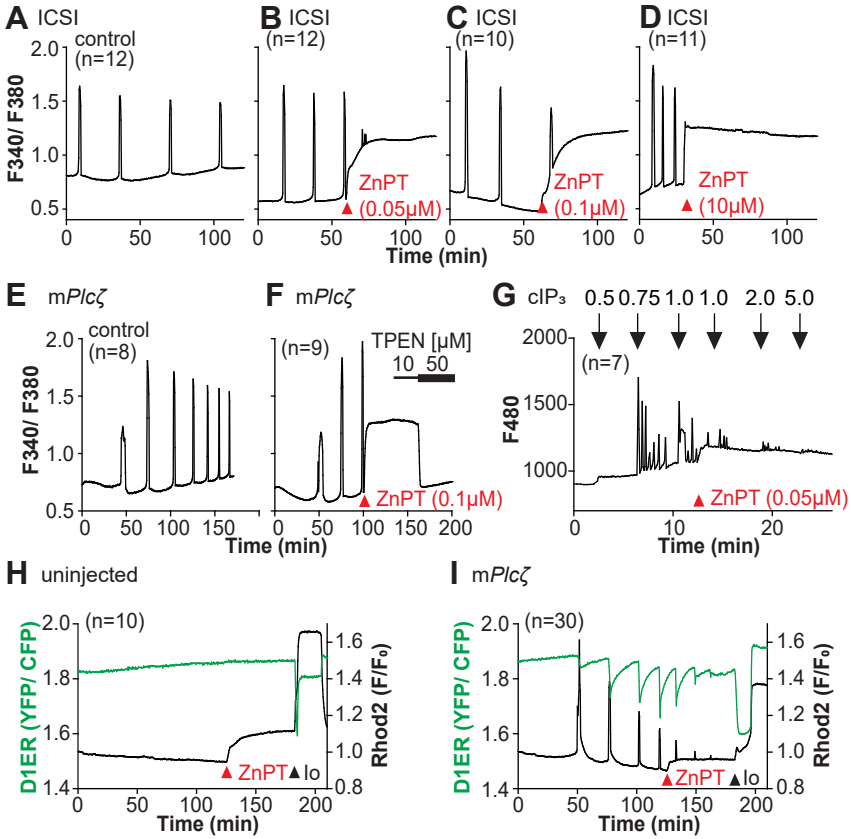
A ICSI
control
(n=12)
F340/ F380
2.0
1.5
1.0
0.5
0
50
100
B ICSI
(n=12)
ZnPT
(0.05μM)
C ICSI
(n=10)
ZnPT
(0.1μM)
D ICSI
(n=11)
ZnPT
(10μM)
Time (min)
E mPlcζ
control
(n=8)
150
F mPlcζ
(n=9)
TPEN [μM]
10 50
ZnPT (0.1μM)
200
G cIP₃
0.5 0.75 1.0 1.0 2.0 5.0
(n=7)
F480
2000
1500
1000
ZnPT (0.05μM)
10
20
H uninjected
(n=10)
D1ER (YFP/ CFP)
Rhod2 (F/F₀)
1.8
1.6
1.4
1.2
0.8
ZnPT
Io
I mPlcζ
(n=30)

Figure 7.

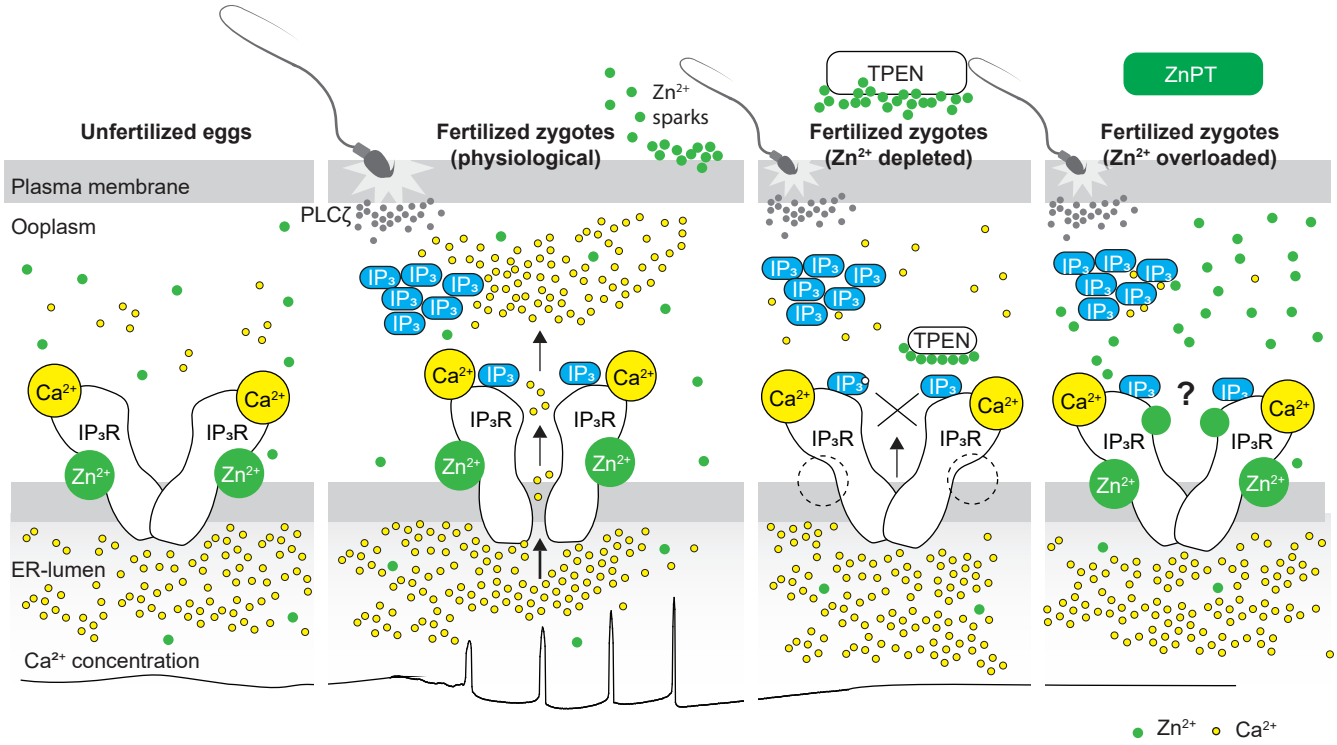
Unfertilized eggs
Fertilized zygotes (physiological)
Fertilized zygotes (Zn^{2+} depleted)
Fertilized zygotes (Zn^{2+} overloaded)
Zn^{2+} sparks
TPEN
ZnPT
Plasma membrane
Ooplasm
PLCζ
IP_3
Ca^{2+}
Zn^{2+}
IP_3R
?
ER-lumen
Ca^{2+} concentration
Zn^{2+}
Ca^{2+}

Supplementary Figure 1.

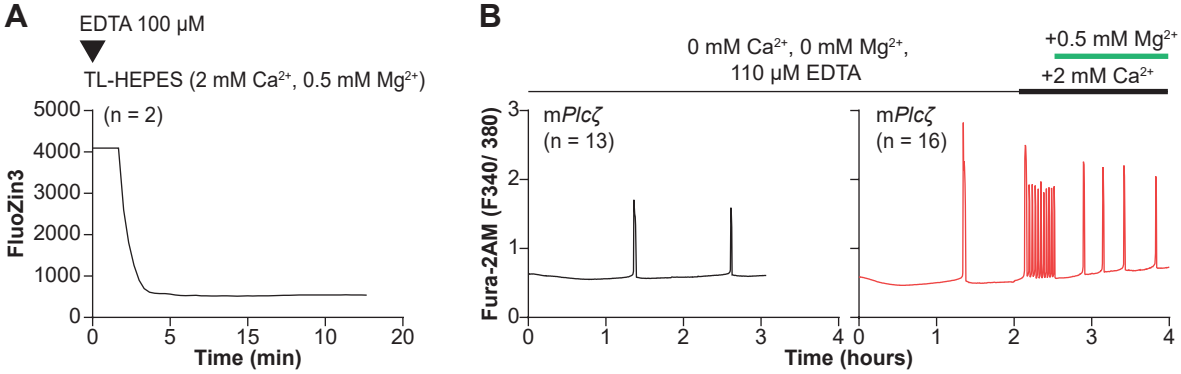

Supplementary Figure 2.

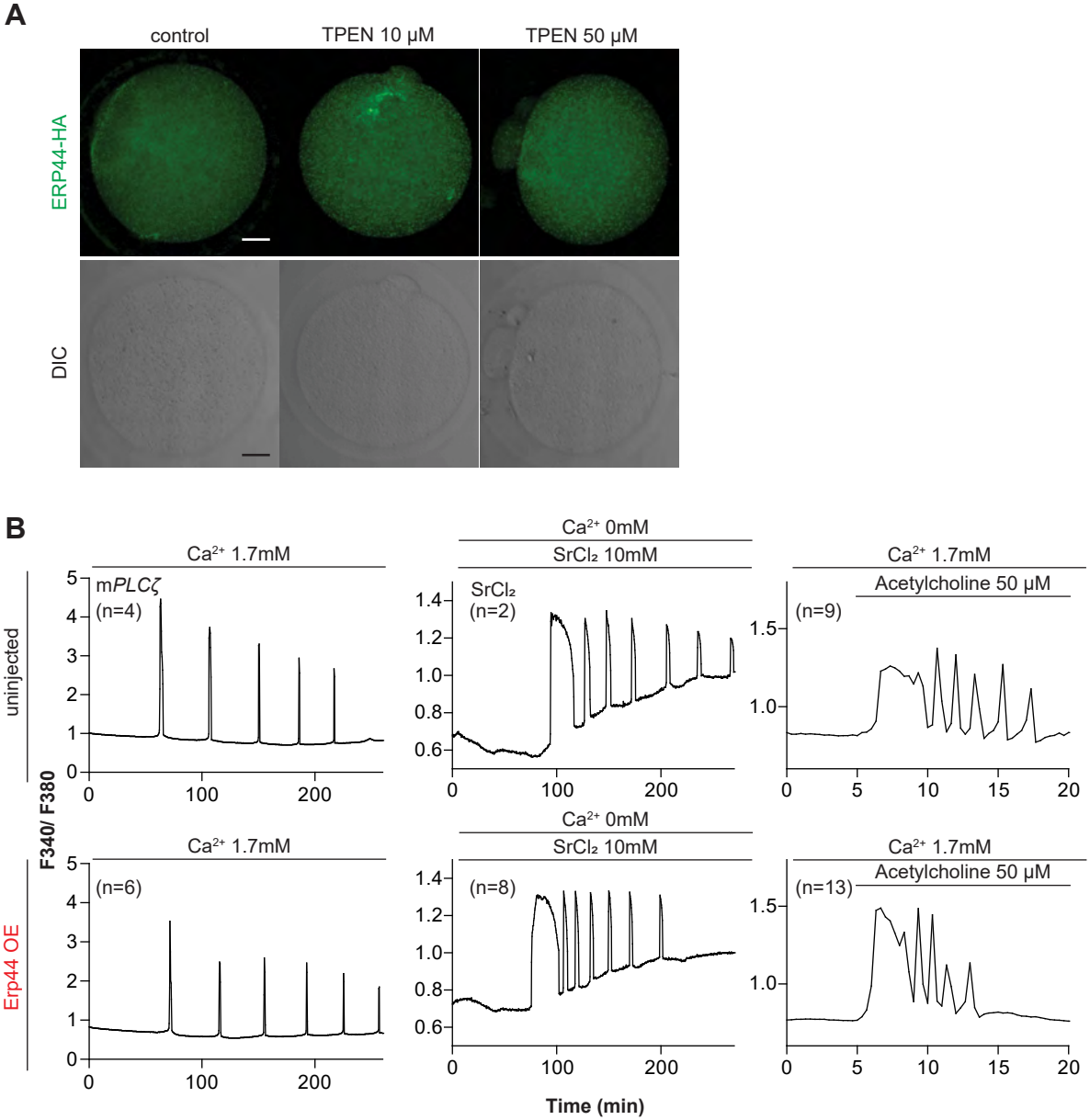
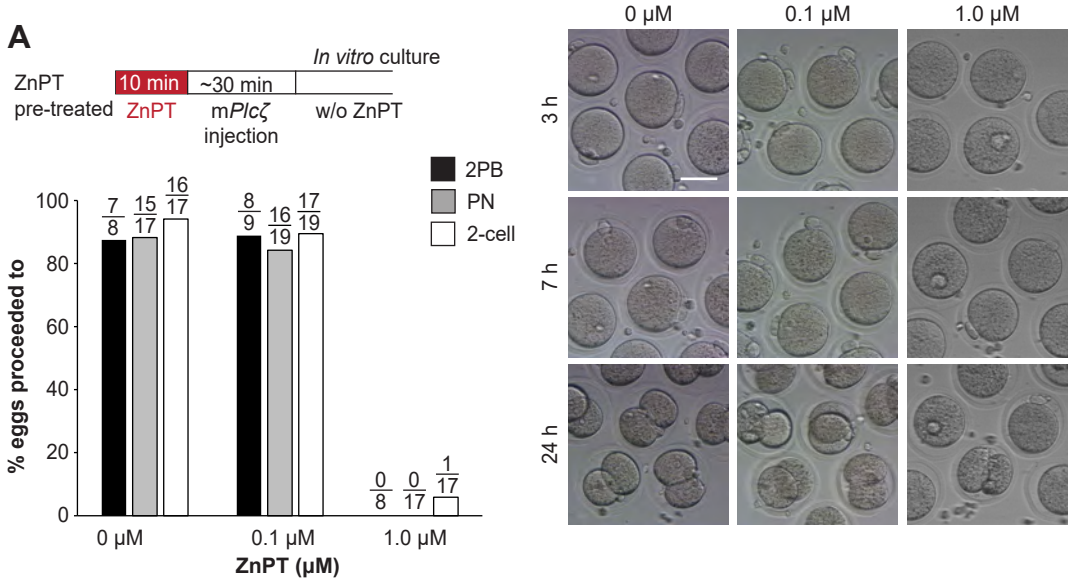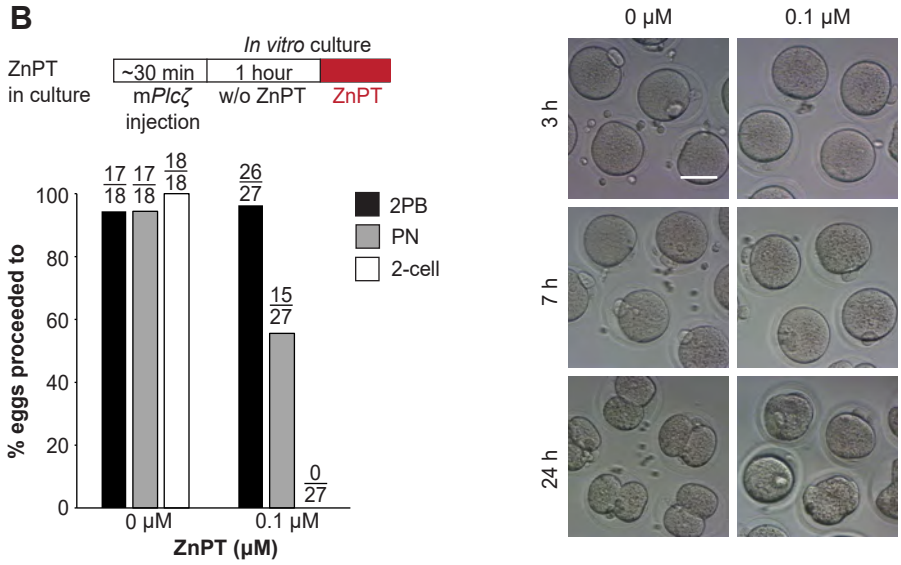
Supplementary Figure 3.